



Multiphase, decoupled faulting in the southern German Molasse Basin — evidence from 3D seismic data

Vladimir Shipilin^{1,2}, David C. Tanner¹, Hartwig von Hartmann¹, and Inga Moeck^{1,2}

¹Leibniz Institute for Applied Geophysics, Stilleweg 2, D-30655 Hannover

²Georg August University Göttingen, Goldschmidtstr. 3, D-37077 Göttingen

Correspondence: Vladimir Shipilin (Vladimir.Shipilin@leibniz-liag.de)

Abstract. We use three-dimensional seismic reflection data from the southern German Molasse Basin to investigate the structural style and evolution of a geometrically decoupled fault network in close proximity to the Alpine deformation front. We recognise two fault arrays that are vertically separated by a clay-rich detachment horizon. A large-scale thrust partially overprints the upper fault array. Analysis of seismic stratigraphy, syn-kinematic strata, throw distribution, and spatial relationships between faults suggest a multiphase fault evolution: (1) initiation of the lower fault array in the Upper Jurassic carbonate platform during the Rupelian, (2) development of the upper fault array in the Cenozoic sediments during the Chattian, and (3) reverse reactivation of the upper faults and thrusting during the mid-Miocene. These phases document the evolution of the stress field during the migration of the forebulge (phase 1), foredeep (phase 2) and the toe of the orogenic front (phase 3) across the investigated area. We postulate that phase 2 was controlled by the vertical stress gradients, whereby a lower horizontal stress component within the Cenozoic sediments defined the independent development of the upper faults above the lower faults. Mechanical behaviour of the clay-rich horizon precluded the subsequent linkage of the fault arrays. A large-scale thrust must have been facilitated by the reverse reactivation of the upper normal faults, as its maximum displacement and extent correlate with the occurrence of these faults. We conclude that the evolving tectonic stresses were the primary mechanism of fault activation, whereas the mechanical stratigraphy and pre-existing structures locally governed the structural style.

1 Introduction

In the last decade, there has been an increasing interest in foreland basins because of the existence of deep aquifers that might host geothermal resources (e.g., Schulz et al., 2004; Weides and Majorowicz, 2014). Understanding of tectonic evolution and fault kinematics is crucial to evaluate potential geothermal reservoirs, which at depths below 3 km are primarily controlled by fault and density of interconnected fractures (Moeck, 2014).

Foreland basins have complex deformation structures that range from normal faults towards the foreland to contractional and inverted faults near the orogenic front (DeCelles and Giles, 1996; Tavani et al., 2015). Such deformation pattern shows that the basin is subject to a variety of stress states that develop during the lithospheric flexuring, subsidence, and sedimentation as the orogenic front progresses forward. Locally, the stress states may be modified by inherited structures, such as pre-existing faults (Tavani et al., 2015; Wibberley et al., 2008), and differences in mechanical behaviour of rock layers (Ferrill et al., 2017).



25 The resultant composite structural history can only be correctly deciphered using a three-dimensional approach, such as can be derived from three-dimensional seismic datasets.

Our working area is within the southernmost part of a typical foreland basin system, the German Molasse Basin, near the town of Geretsried, 30 km south of Munich (Fig. 1). A number of basin-scale structural studies were carried out in the '80s and '90s, based on a large amount of 2D seismic data acquired for hydrocarbon exploration over decades (e.g., Bachmann et al., 1982, 1987; Müller et al., 1988; Bachmann and Müller, 1982). The increasing interest in geothermal exploitation in recent years and therefore the acquisition of 3D seismic data, have allowed more detailed studies of the complexly deformed areas (e.g., Lüschen et al., 2011; von Hartmann et al., 2016; Budach et al., 2017). Nevertheless, the tectonic and stratigraphic factors controlling the evolution of the structure of the German Molasse Basin have not been fully described as yet.

35 The focus of this work is an in-depth analysis of deformation structures in the Geretsried study area. Our aim is to understand the complex structure and tectonic evolution of an area proximal to the Alpine deformation front. To achieve this, we use 3D seismic reflection data to (i) reconstruct the temporal and spatial evolution of the fault network within the Molasse sequence and its Mesozoic substratum, and (ii) evaluate the impact of the evolving stress field, pre-existing deformation structures, and mechanical stratigraphy on fault evolution, structural style, and kinematic interactions between faults.

2 Geological Setting

40 The German Molasse Basin (GMB) is part of the North Alpine Foreland Basin (Figs. 1 and 2) that evolved on the subducting European margin, in front of the Alps, since the Late Eocene (Lemcke, 1973; Bachmann et al., 1982). The Cenozoic deposits of the foreland basin unconformably overlie the peneplained Mesozoic sedimentary basement (Fig. 3) and locally, Permo-Carboniferous clastic sediments and crystalline rocks (Lemcke, 1973; Sissingh, 1997).

From Jurassic to mid Cretaceous, the region of the future Molasse Basin evolved as a proximal passive margin (Frisch, 1979; Ziegler, 1990; Pfiffner, 1992). Submergence of the southern European shelf by the Tethys Ocean in the Jurassic led to the deposition of Lower and Middle Jurassic marine shales and the establishment of an Upper Jurassic carbonate platform (Meyer & Schmidt-Kaler, 1990). In the southeast, the carbonate platform is overlain by partially preserved, Cretaceous, shallow-water carbonates and deep-water marls and shales (Fig. 3; Bachmann et al., 1987).

After a profound hiatus in sedimentation caused by the Late Cretaceous-Palaeocene contractional event as consequence of the change in the African plate motion (Kley and Voigt, 2015), deposition resumed in the Late Eocene (Ziegler et al., 1995; Sissingh, 1997). It marks the inception of the foreland basin in response to the Euro-Adriatic collision (Frisch, 1979; Allen et al., 1991; Ziegler et al., 1995). Loading and consequent flexure of the European foreland plate created a wedge-shaped basin fill (Allen et al., 1991). Flexural subsidence was accompanied by the formation of longitudinal (i.e., foredeep-parallel) normal faults (Lemcke, 1988; Bachmann et al., 1982; Bachmann and Müller, 1982).

55 The Cenozoic Molasse cover was deposited in the course of two major transgressive-regressive cycles and can be subdivided into, from older to younger; the Lower Marine Molasse (Untere Meeresmolasse, UMM), the Lower Freshwater Molasse (Untere Süßwassermolasse, USM), the Upper Marine Molasse (Obere Meeresmolasse, OMM), and the Upper Freshwater Molasse



(Obere Süßwassermolasse, OSM) (Figs. 2 & 3; von Guembel, 1861). The UMM is Late Eocene to Early Oligocene in age and consists of transgressive sandstones, shelf carbonates, and deep-water shales and marls (Lemcke, 1988; Sissingh, 1997). The
60 Mid-Oligocene accumulation of regressive, shallow-marine to coastal Baustein sandstones marks the transition from UMM to USM (Diem, 1986). These are overlain by fluvial Chattian and Aquitanian sandstones.

In Early to Middle Miocene times, thrusting of the Alps abated and subsidence rates decreased (Zweigel, 1998). Despite decreasing subsidence, the second transgressive-regressive cycle began in the Burdigalian with transgression of OMM marls over the Aquitanian-Burdigalian unconformity (Fig. 3; Lemcke, 1988; Zweigel, 1998). At the same time, the basin-infill geometry
65 changed from wedge-shaped to tabular (Fig. 2; Kuhlemann and Kempf, 2002). This suggests that the foreland plate was not affected by further flexure and that the marine transgression during the deposition of OMM was the result of lower sediment input into the basin (Zweigel, 1998; Kuhlemann and Kempf, 2002; Ortner et al., 2015). By the beginning of the Langhian, terrestrial conditions prevailed across the entire GMB, as the OSM was deposited (Lemcke, 1988).

At the southern basin margin, the Folded (Subalpine) Molasse was formed by thrusting and incorporation of the proximal
70 foreland basin sediments into the Alpine front (Fig. 2; Bachmann et al., 1987; Reinecker et al., 2010; Ortner et al., 2015). Thermochronological data suggest that the thrusting in the Folded Molasse continued into the Late Miocene (von Hagke et al., 2015). From c. 8.5 Ma onwards, the GMB experienced isostatically-induced uplift and erosion (Lemcke, 1973).

3 Database

The main database for this investigation is a Kirchhoff pre-stack, depth-migrated, 3D seismic reflection survey. It was acquired
75 in 2010 for geothermal exploration and covers an area of c. 40 km² in the southern part of the GMB (Fig. 1). The seismic volume has a record length of 5000 ms two-way travel time (TWT) with a 36-fold bin size of 25 m by 25 m. It is displayed with SEG standard polarity; that is, positive and negative impedance contrasts are depicted as peaks (red) and troughs (blue), respectively. The vertical stratigraphic resolution ranges from c. 20 m within the Cenozoic Molasse sediments to c. 55 m at the base of the carbonate platform. Additionally, we used paper copies of two c. 7 km long seismic profiles that were acquired
80 in 1987 to investigate the deformation style at the transition between the Foreland Molasse and the Folded Molasse. The profiles are located south and southeast of the 3D seismic survey area (Fig. 1b) and therefore allowed us also to investigate the southward extent of the structures identified within the 3D seismic survey.

The seismic reflection data are supplemented by a vertical seismic profile and formation top data from the only borehole available within the study area — GEN-1, down to the intermediate level of the Upper Jurassic carbonate platform (Fig. 3). We
85 used time-to-depth picks obtained from the vertical seismic profile to calibrate the interval migration velocities. The resultant velocity model was used for time-to-depth conversion.



4 Methodology

4.1 3D seismic interpretation

The 3D seismic reflection survey was interpreted in the time domain using Schlumberger Petrel® seismic interpretation software. We used the vertical seismic profile data to tie well stratigraphy to the seismic dataset. This provided age constraints for seven seismic horizons that were mapped across the dataset from the top of the Purbeckian limestone, which corresponds to the top Berriasian, up to the highest seismically recognizable horizon — top Aquitanian (Fig. 3). An additional horizon — the inferred base of the carbonate platform (top Callovian) — was also interpreted. For this interval, there is no well control and vertical seismic resolution is poor. We picked a prominent positive-phase reflection that can be considered the base of the carbonate platform, given the reported 600–650 m thickness of the latter (Lemcke, 1988), and expected strong acoustic impedance contrast due to a change in lithology, and therefore velocity and density, from the Upper Jurassic carbonates to the Middle Jurassic clastics.

To better detect faults, we implemented a fault enhancement filter to the seismic dataset and used seismic volume attributes, such as variance and curvature. The fault enhancement filter suppresses random noise and enhances amplitudes at fault locations, resulting in sharper fault edges. Hence, high variance anomalies became more pronounced, highlighting faults that have discrete offsets. The curvature attribute was used to infer the presence of faults where a discrete offset is succeeded by a ‘curved’ reflection shape. Such curved geometries could be the seismic expression of subseismic conjugate faulting, plastic deformation in the presence of mechanical stratigraphy, or an imaging artefact due to lateral changes of seismic velocities at faults (Marfurt, 2018).

Subsequently, the variance and curvature volumes were co-rendered to map the full extent of the faults. The faults were traced on time-slices in multiattribute display and then mapped on vertical sections in reflectivity display. The vertical sections were preferentially oriented perpendicular to the strike of the faults, with a line spacing of 75–100 m.

4.2 Structural Modelling

In addition to 3D seismic interpretation of key stratigraphic horizons and faults, we created a consistent 3D structural model to analyse the three-dimensional relationship between faults and sedimentation. For the modelling, the interpreted stratigraphic horizons and faults were depth-converted and imported as ASCII point-sets into SKUA-GOCAD® (Paradigm Ltd., 2017). We used two interpolation methods to construct triangulated surfaces from point-sets; (i) direct triangulation for fault modelling, and (ii) discrete smooth interpolation for stratigraphic surface modelling. The former method directly tessellates the surfaces, whereby the interpreted points are used as hard constraints to form the vertices of triangles. In the latter method, the interpreted points are not directly part of the surface. Instead, the discrete smooth interpolation creates a trend surface, whereby the interpreted points are honoured as soft constraints in a least-square sense (Mallet, 2002). The resultant surface has a minimum distance to the points and is therefore representative of the original interpretation. We chose the latter method for stratigraphic horizon modelling, because it minimises the artificial roughness of the surfaces, which is inherited from the interpretation



120 due to a large amount of data points. To model displacement of stratigraphic horizons along faults, we used the ‘Modelling
Horizon-to-Fault Contacts’ module in the ‘Structural Modelling’ workflow. It consists of two steps:

1. Calculation of a horizon-to-fault contact line between the current geometry of the horizon and the fault. New irregularly spaced points are created within the horizon surface, along the contact with the fault.
- 125 2. Construction of a faulted horizon. The horizon surface is opened along the fault plane using the discrete smoothing interpolation algorithm. The original point-set is used as control points to allow the interpolation algorithm to keep the faulted horizon as close as possible to the original point-set. Points within the vicinity to the fault are considered of a high interpretation uncertainty and therefore we excluded the points within 50 m of the fault from the interpolation process.

From the structural model, we used the following tools to obtain temporal and spatial constraints on the evolution of the investigated fault network:

130 (i) Isochore maps of the key stratigraphic units. This tool allows us to analyse thickness variations across faults to infer their syn-depositional activity (e.g., Jackson and Larsen, 2009; Tvedt et al., 2013; Ziesch et al., 2017). The isochore maps were generated by computing vertical distance between the modelled horizon surfaces bounding a stratigraphic unit and projecting this information (as a scalar value at every triangle node) onto the basal horizon. The algorithm calculates the vertical distance from the basal horizon surface to the nearest top horizon surface, so that overlapping of surfaces due to contractional faulting
135 does not produce an artefact. The major limitation of this method are the computational artifacts associated with the gaps on the top surface produced by normal faults. The computational algorithm attributes zero values to the area of the basal horizon surface directly beneath the fault gap and interpolates minimal values to the adjacent regions to avoid abrupt thickness change to zero meters. This results in significant thinning of a stratigraphic unit towards a fault, which is in fact a computational error.

(ii) Juxtaposition (Allan) diagrams. These diagrams show the throw distribution in a view parallel to the fault surface and
140 therefore provide insight into the growth and linkage history of the fault (Allan, 1989). A juxtaposition diagram is constructed by projecting fault cut-offs of the stratigraphic horizons onto a vertical plane that is perpendicular to the pole of the fault surface. To quantify throw distribution, we created polylines at fault cut-offs with nodes at a constant interval of 50 m and plotted them onto depth vs. fault strike-length diagram. Additionally, we produced vertical throw distribution plots (t-z plots) for selected faults to quantify their growth and propagation (e.g., Cartwright et al., 1998; Baudon and Cartwright, 2008a, b, c;
145 Tvedt et al., 2013).

(iii) Stereographic projections of the poles of fault surfaces to characterise the geometry of the faults (von Hartmann et al., 2016; Ziesch et al., 2017).



5 Results

5.1 Seismic stratigraphy

150 The good quality of the seismic data, along with the lithological constraints of the mapped horizons enabled us to establish a seismic-stratigraphic framework of the study area, and characterise depositional patterns of the basin fill. The identified horizons define seven seismic-stratigraphic units as shown on the representative seismic profiles in Figures 4, 5, and 6. The stratigraphic framework (Fig. 3) qualitatively depicts the mechanical stratigraphy of the identified units, providing information on the competence contrast rather than actual rock strength. The latter is difficult to assess for rocks at the time they were
155 deformed (Ferrill et al., 2017). The stratigraphic units are specified as either competent or incompetent, based on the published interpretation of their mechanical behaviour from outcrop and well data (Fischer, 1960; Müller, 1970; Budach et al., 2017) and on the mechanical properties from literature, e.g., von Hartmann et al. (2016). Figure 3 shows also inferred locations of detachment horizons (Bachmann et al., 1982; Müller et al., 1988; Ortner et al., 2015; von Hartmann et al., 2016).

Unit 1 has a heterogeneous, low-frequency seismic expression that corresponds to the Upper Jurassic carbonate platform.
160 Seismic patterns in its lower part are characterised by c. 150 m thick relatively continuous, moderate-amplitude reflections, whereas seismic patterns in the middle and upper parts exhibit alternating chaotic to sub-parallel, low to moderate-amplitude reflectivity. The base of the unit is marked by a low frequency, locally incoherent reflection interpreted as top Callovian. In contrast, the upper-bounding reflection, top Berriasian, is generally continuous and easy to correlate even when extensively faulted.

165 Units 2 and 3 constitute a package of continuous, low-frequency, and high-amplitude seismic events that reflect contrasting lithologies. Unit 2 corresponds to mechanically incompetent Cretaceous shales and marls and a thin layer of sandstone, whereas Unit 3 represents competent Priabonian sediments (Basal sandstone and Lithothamnion limestone) (Budach et al., 2017). Unit 2 thickens substantially southwards (from c. 90 m to c. 170 m), which is in agreement with the regional northward-oriented truncation of the Cretaceous sediments. In contrast, Unit 3 only slightly thickens to the south.

170 Low amplitude, semi-continuous reflections of Unit 4 onlap onto the upper boundary of Unit 3 — top Priabonian. It is the most prominent reflection across the survey marking an abrupt change from shallow-marine to deep-marine sedimentation during the Rupelian. It also marks the transition from the competent Unit 3 to an incompetent Unit 4 (Fischer, 1960; Müller, 1970; Budach et al., 2017; von Hartmann et al., 2016). Poor reflectivity of Unit 4 is explained by low impedance contrast within the Rupelian clays and marls. At the top, the unit is marked by toplap terminations below a continuous, moderate-amplitude
175 negative reflection — top Rupelian (Fig. 5). The unit shows a profound thickness increase from c. 600 m in the north to c. 800 m in the south.

Unit 5 is characterised by parallel, highly continuous and high amplitude reflections that correspond to more competent Baustein beds (Budach et al., 2017). Strong impedance contrasts within the unit are attributed to interlayering of sandstones and marls. Unit 5 has a uniform stratigraphic thickness across the survey.

180 Unit 6 overlies Unit 5 in a concordant manner. While its lowest part has similar reflection characteristics to Unit 5, reflectivity and continuity of seismic events of the middle part decrease upwards. This is due to the increasing marl content, as



evidenced by the GEN-1 well (Fig. 3). Thus, mechanical competence of the unit also decreases upwards. The uppermost part of the unit is characterised by continuous, high-amplitude reflections, which are caused by sandstone-marl alternations. To the south, bedding changes dip direction from southward to northward due to the folding-related deformation. Unit 6 increases in thickness to the south, giving it a wedge-shape geometry.

The seismic response of Unit 7 consists of moderately continuous, low to moderate amplitude reflections. The frequency of the seismic events increases upward within the unit. It corresponds to the Aquitanian sandstone-marlstone series that show no thickness change.

5.2 Structural framework

The 3D structural model shows that the study area contains two distinct fault arrays that are geometrically (vertically) decoupled and a large thrust (Fig. 7). We term these decoupled fault arrays the lower and the upper. In the former, faults do not extent upwards beyond clay-rich Unit 4, and in the latter, faults terminate downwards within Unit 4 (Fig. 4). The geometry and distribution of the lower faults is depicted on the multiattribute and depth-structure maps of top Turonian (Figs. 8a, b), while the geometry and distribution of the upper faults is depicted on the multiattribute and depth-structure maps of top Rupelian (Figs. 8c, d) and top Baustein beds (Figs. 8e, f). The strike direction of the thrust is shown on the multiattribute and depth-structure maps of top Baustein beds (Figs. 8e, f).

5.2.1 Lower fault array

The lower fault array consists of normal faults that are parallel with respect to the Alpine deformation front, striking WSW–ENE or W–E and dipping either towards the orogen (synthetic faults) or the foreland (antithetic faults) (Figs. 8a,b, and Fig. 9). In cross-section, the majority of the faults appear planar and dip 75° to 85° , except for the listric faults Gartenberg S and Gartenberg N that have shallower dip angles of 60° to 65° (Figs. 4 and 6) already in the upper section of the reservoir, which further decrease with depth.

With respect to their vertical extent and the stratigraphy they displace, the lower faults are subdivided, for descriptive purposes, into major and minor faults. The major faults offset crystalline basement and tip-out upward into Unit 4 (Rupelian) (e.g., Fault Gelting N, Fault NE), where the Rupelian reflections blanket the fault tips (Figs. 4, 9, 10). In contrast, the minor faults show no discernible offset of the basement and tip-out upward within either Unit 2 (Cretaceous) or lowermost Unit 4 (Rupelian). The tips of the minor faults that do not breach Unit 2 (Cretaceous) are overlain by monoclines (Fig. 4).

Two prominent graben structures in the NW and centre of the study area are defined by major conjugate faults (Fig. 7a, b). The largest displacement across the NW graben is accommodated on the NW-dipping master fault, Fault Gelting N, with c. 150 m of throw at top Berriasian. Displacement along the northern flank of this graben is distributed across SE- and S-dipping, conjugate and secondary, antithetic faults. In contrast, the central graben switches its polarity (i.e., controlling fault) from the northern boundary fault, Fault Gartenberg N, to the southern boundary fault, Fault Gartenberg S. In the western segment, the maximum displacement of c. 120 m is accrued at top Berriasian on the former fault, whereas in the eastern segment, the largest displacement of c. 150 m at top Berriasian is accrued on Fault Gartenberg S. The switch of the graben polarity is also



215 expressed by the presence of the rollover anticlines in the graben interior; in the west, there is a rollover anticline towards Fault Gartenberg N (Fig. 4), whereas in the east the rollover anticline is towards Fault Gartenberg S (Fig. 9). The bounding faults of the central graben have no displacement at top Callovian. The along-strike seismic section (Fig. 5) through the central graben clearly shows thinning of Unit 1 (Upper Jurassic) within the graben.

5.2.2 Upper fault array

220 The upper fault array exhibits reverse faulting geometries in the central and northern parts of the study area — Cenozoic (CZ) reverse faults 1, 2, 3, and 4 (Figs. 7, 8d,f) and normal faulting geometries in the southern part — Cenozoic (CZ) normal faults (Figs. 7, 8d). The upper faults strike approximately in the same direction as the lower faults, and show considerable lateral offset with respect to their lower counterparts (Fig. 12). The lateral extent of the upper faults does not correlate with the lateral extent of the lower faults (Fig. 12). Like the lower faults, the upper faults have alternating dip directions; they dip either to the
225 S or to the N (Fig. 7, 8d,f), often showing opposing dip with respect to each other. The dip angles of the CZ reverse faults range from 50° to 60°, whereas the CZ faults showing normal fault geometry dip steeper — 65° to 70°.

The upper faults offset the mechanically competent Unit 5 (Baustein beds) and die out upwards in Unit 6 (Chattian) and extend downwards into Unit 4 (Rupelian) (Figs. 4 and 6), where the observation of internal deformation is hindered by the semi-transparent reflections. The CZ reverse faults have low throw magnitudes that do not exceed 50 m at both top Rupelian
230 and top Baustein beds. In contrast, the CZ faults with normal fault geometry reach maximum throw values at top Rupelian that are twice that of the reverse faults (c. 100 m; Fig. 8d).

5.2.3 Thrust faults

The normal faults of the upper fault array are overprinted by the extensive Geretsried Thrust that dips 20° to 35° to the S and has two branches. Its stratigraphically higher upper branch thrust dips parallel to the lower master thrust within Unit 6
235 (Chattian) (Fig. 10). Both thrust faults terminate with ramps within Unit 6 (Chattian) — no upper detachment is observed.

To understand the evolution of the thrust faults that dominate the deformation pattern of the Cenozoic sequence in the southern part of the study area, we investigated their geometries, up to the Kirchbichl Thrust, the frontal thrust of the Folded Molasse. The seismic profiles A and B (Figs. 10 and 11, resp.), depict the southward continuation of the Geretsried Thrust. They also illustrate the overall tectonic style at the northern tip of the Alpine orogen, which is dominated by a simple overthrust
240 (the Kirchbichl Thrust) with a minor triangle zone in its footwall. At the foot of the thrust, the Cenozoic sediments are tilted to the N to a varying extent, as shown in the profiles A and B.

In the western profile A (Fig. 10), the Geretsried Thrust emanates from a basal décollement below the carbonate platform, c. 4 km south of the study area, and truncates both the Mesozoic and Cenozoic units over a distance of c. 7 km, dying out in the upper part of Unit 6 (Chattian). An upper thrust branches from the main Geretsried Thrust within Unit 4 (Rupelian), with
245 a steeper dip (c. 45°) within Unit 5. The flat-ramp geometry of the Geretsried Thrust creates a distinct NNW-verging hanging-wall anticline — the Geretsried Fold. Where the Geretsried Thrust steps over the linkage zone, i.e., relay ramp, between the two CZ normal faults, the core of the Geretsried Fold is extensively deformed by back-thrusts and a shallow-dipping reverse



fault that accommodate shortening of Units 5 and 6 (Figs. 4, 6). Here, the thrust dips steeper (c. 35°) (Fig. 13) and the fold core exhibits typical asymmetry, with a narrower forelimb and a broader, shallow-dipping backlimb.

250 In the eastern profile B (Fig. 11), the Geretsried Thrust likewise ramps up from the basement into the carbonate platform, but terminates already within Unit 4. There is no thrust-related folding above the Geretsried Thrust beyond Unit 4. Notably in this profile, the Cenozoic Molasse sediments are tilted to the N to a much greater extent than in the western profile, where the Geretsried Thrust propagated further into the foreland.

5.3 Structural analysis of selected faults

255 To infer the syn-depositional activity of the interpreted faults, we analysed thickness variations of the seismic-stratigraphic units using isochore maps (Fig. 14). Unit 1 in Figure 14a displays no significant thickness variation across major faults that offset the basement. However, it shows slight thinning of hanging-wall blocks of minor faults that do not reach into the basement. Isochore map in Figure 14b shows no consistent thickening of Unit 2 across all major faults. There are however local thickness variations in form of footwall thinning and hanging-wall thickening across Fault Gartenberg S, eastern segment of Fault NE
260 and Fault Gartenberg N, and the central segment of Fault Gelting N. In the south, local depocentres are observed in Unit 2 that are not related to fault activity. Unit 3 thickens only across Fault Gartenberg N (Fig. 14c). In contrast to the underlying units, the Rupelian clays of Unit 4 clearly exhibit a syn-kinematic nature, particularly where faults emerge from the carbonate platform (Fig. 14d). This is especially evident within the central and the NE grabens, where the Rupelian strata is thicker than to the north or south of the graben-bounding faults. Furthermore, we observe onlapping of the Rupelian reflections onto
265 the top Priabonian reflection in the easternmost margin of the graben (Fig. 5). In the southeastern part, there is a profound thickness decrease of Unit 4 associated with downthrow of the hanging-wall blocks of the upper CZ normal faults (Fig. 14d). Unit 5 displays no thickness variations across upper faults, except in the southeast, where it is thickened by displacement on the Geretsried Upper Thrust (Fig. 14e). Although Unit 6 in Figure 14f continuously thickens towards the S, it thins within the hanging-wall anticline (i.e., the Geretsried Fold).

270 Figures 15, 16 and 17 depict Allan maps and throw-depth diagrams of faults NE, Gartenberg S, and Gelting N, respectively, that are used to specify the temporal evolution of the lower faults. Fault NE is fully imaged by the seismic data. This allows us to document the geometry of its tip lines at the lateral terminations. The tip lines converge up- and down-dip from top Berriasian and must eventually meet within Unit 4 and the basement, correspondingly (Fig. 15a). The largest throw is located at top Berriasian (c. 100 m, as shown in profile 3), from which it decreases both up- and downwards (Fig. 15b). The upward
275 decrease of throw is gradual in profiles 1 and 2, whereas in profiles 3 and 4, throw minima are observed (Fig. 15b). These correspond to the local thinning and thickening of Unit 2 (Turonian) at the eastern segment of the fault plane (Fig. 14b). Fault Gartenberg S has no detectable throw at top Callovian, so only three cut-off polygons are available for the throw analysis (Fig. 16a). Similar to Fault NE, the lateral extent of Fault Gartenberg S decreases up-dip and the fault throw is the largest at top Berriasian. All throw minima are located at top Turonian on *t-z* profiles (Fig. 16b). For Fault Gelting N it is more difficult
280 to establish a distinct trend of throw distribution (Fig. 17). This could be due to the overall poorer image quality at the fault region, which introduced uncertainty in cut-off picking, especially at top Callovian. Generally, the throw on Fault Gelting N is



distributed equally from top Callovian to top Priabonian, with a minor throw reduction at top Turonian (Fig. 17b). As shown in the t - z plot (Fig. 17b), the throw values vary mostly only by c. 25 m.

285 A map of the cut-off lines at top Baustein beds depicts the lateral distribution of throw on the Geretsried Thrust (Fig. 18). The thrust rapidly loses throw to the east: from c. 250 m in the westernmost extent of the survey area to the negative throw values of c. 50 m in the easternmost extent. The negative throw values are presumably the result of the residual slip on the pre-existing CZ normal faults that were not completely reversed. Similarly, the upper branch of the Geretsried Thrust dies out to the east within the study area. The loss of displacement on the thrust faults is reflected by the eastward termination of the Geretsried Fold (Fig. 19). Due to poor resolution of the uppermost part of the seismic volume recognition of growth strata
290 above the Geretsried Fold is not possible.

6 Discussion

The deformation pattern in our study area is characterised by two geometrically decoupled fault arrays with both normal and reverse sense of slip and through-going thrust faults. Such a deformation pattern documents three distinct phases of faulting activity, which implies a paleostress change during the evolution of the foreland basin. In this section, we interpret our observations on reflection configuration, fault throw distribution, stratal thickness variations, and spatial relationships between
295 faults to describe the temporal and spatial evolution of the faults in the Geretsried area. Furthermore, we discuss the governing factors on the evolution of the fault network that defined the present-day deformation pattern, such as evolving stress states, pre-existing deformation structures and mechanical stratigraphy.

6.1 Temporal and spatial evolution of the fault network

300 Structural analysis suggests that the investigated fault network evolved in three phases: (1) normal faulting in the early Rupelian, (2) normal faulting in the Chattian, and (3) reverse and thrust faulting in the mid-Miocene.

The first faulting phase occurred in the early Rupelian and resulted in the formation of the lower fault array. Two lines of stratigraphic evidence provide time constraints for the lower fault activity; (1) substantial thickening of the syn-orogenic Rupelian strata across faults (Fig. 14d), and (2) onlap and discordant patterns of the Rupelian reflections within the hanging-
305 wall blocks (e.g., Fig. 5). Faulting activity ceased before the sedimentation of Rupelian was complete, as the fault tips are covered by the Rupelian reflections and there is no apparent offset at top Rupelian (Figs. 4, 6, and 10). These findings are in accordance with the works of Bachmann and Müller (1991) and Sissingh (1997), who report Priabonian to Rupelian syn-sedimentary faulting in the southern part of the GMB, based on the interpretation of regional seismic profiles.

The upper faults with reverse sense of slip most probably formed as normal faults, as suggested by their strike (i.e., WSW–
310 ENE strike) and steep dips. The absence of geometrical coupling between the lower and upper faults and their overall distinct geometries (e.g., varying lengths, considerable lateral offset, opposite dip directions), indicate that the latter faults developed independently from the former faults, in the shallower Cenozoic level. We infer that they developed during the second faulting phase in the Chattian. The evidence, such as (1) limited thickness variations across faults in the Baustein strata (Fig. 14d),



and (2) termination of the fault tips within the Chattian strata (Figs. 4 and 6), shows that the upper faults initiated after the
315 deposition of the Baustein beds (Unit 5), and were syn-sedimentary during deposition of the Chattian sandstones (Unit 6).

The third faulting phase is signified by the reverse reactivation of the upper normal faults, development of the Geretsried
thrust, and thrust-related folding in the mid-Miocene times. Due to the resolution limit in the upper part of the 3D seismic cube,
it was impossible to recognise growth strata above the Geretsried Fold that could provide age constraints for the contractional
deformation. However, we hypothesise that the Geretsried thrust was contemporaneous with or succeeded the frontal thrusts
320 of the Folded Molasse, because it is rooted below the Folded Molasse and is thus kinematically related to the frontal thrusts.
This implies a forward-propagating Alpine thrust system, which is most likely. The documented age of the growth strata within
the tilted footwall of the Kirchbichl Thrust indicates that the contractional deformation started in the Badenian (Unger, 1989;
Ortner et al., 2015).

6.2 Controlling factors on fault evolution in the southern GMB

325 6.2.1 Stress field evolution

The temporal and spatial evolution of the deformation structures in the Geretsried area are primarily controlled by the evolving
stress states. Each of the identified faulting phases marks the changes in the regional stress field triggered by the migration of
the forebulge and foredeep across the study area, as the Alpine front propagated northwards.

The first faulting phase was triggered by the flexure-induced extensional stress field. It has been recognised that during
330 foreland flexuring, the upper and lower parts of the bending plate experience extension and compression, respectively, whereas
a central horizon is neutral (Turcotte and Schubert, 1999; Price and Cosgrove, 1990). Within the region of maximum flexure,
elastic bending facilitates an extensional stress field with the negative effective minimum stress oriented perpendicular to the
trend of the foredeep (Bradley and Kidd, 1991; Bachmann and Müller, 1982; Londoño and Lorenzo, 2004; Langhi et al., 2011;
Tavani et al., 2015; von Hartmann et al., 2016). Consequently, normal faults form, striking parallel to the trend of the foredeep.
335 The WSW–ENE and W–E strike of the lower faults is consistent with the transient extensional stress field that must have
existed in the Molasse Basin due to the northward propagation of the flexural front. We thus infer that the lower fault activity
initiated as the forebulge, the region of maximum flexure, reached the Geretsried area in the early Rupelian. With the ongoing
propagation of the Alpine thrusts onto the foreland, the effective minimum stress eventually attained positive values, which
resulted in termination of normal faulting in the late Rupelian.

340 Renewed tectonic activity in the foreland basin, signified by the development of the upper normal faults within the Cenozoic
Molasse sequence, indicates that a normal faulting stress regime was established at this stratigraphic level. The longitudinal
strike of the upper faults implies that the established stress regime was caused by the same tectonics that triggered lower
faulting — the Cenozoic foreland flexure. By the Chattian times, the foreland foredeep approached the study area, as is evident
from the southward thickness increase of Unit 6 (Chattian) (Fig. 14f). This resulted in the onset of rapid sedimentation, as
345 confirmed by the sequence-stratigraphic investigations (Jin et al., 1995; Zweigel, 1998) and the studies on pressure distribution



(Müller et al., 1988; Müller and Nieberding, 1996) in the southern part of the GMB. Increasing sedimentary load towards the orogen produced an increase in the vertical stress magnitude (Drews et al., 2018) and therefore favoured normal faulting.

While the increase of the vertical component of the stress field triggers normal faulting, the vertical gradient of the horizontal component, oriented perpendicular to the trend of the foredeep, governs the position of fault initiation. Due to the ongoing
350 flexuring in the Chattian, the horizontal stress magnitude within the foredeep is expected to be smaller at shallower stratigraphic levels and conversely larger at deeper stratigraphic levels. The numerical model of stress in the Molasse Basin by von Hartmann et al. (2016) confirms the existence of the vertical stress gradients within the basin fill during the Cenozoic flexuring. We therefore explain the independent development of the upper fault array in the shallower Cenozoic by lower magnitudes of the horizontal stress component that existed at this interval and acted perpendicular to the planes of the longitudinal faults. The
355 horizontal stress component must have been the least principal stress for the normal faulting to initiate.

Reverse reactivation of the upper normal faults, thrusting and folding deformation during the third faulting phase point to a stress regime, in which the magnitude of the horizontal stress component, oriented parallel to the shortening direction, exceeded the magnitude of the vertical stress component. Such stress field configuration must have been established in the mid-Miocene as the Alpine thrust wedge approached the study area. The N–S directed shortening must have been first accommodated by the
360 reverse reactivation of the longitudinal upper normal faults due to their inherited low-cohesion and favourable orientation, and then eventually by the development of new thrusts.

6.2.2 Pre-existing structures

Inherited deformation structures have been recognised as influencing structural style, i.e., kinematic and geometrical interaction between faults in the foreland settings (e.g., Butler, 1989; Scisciani et al., 2001; Bry et al., 2004; Calamita et al., 2012; Tavani
365 et al., 2015). In this subsection, we attempt to shed light on the following two questions:

1. Did any the lower fault array develop from the pre-existing pre-orogenic faults?
2. What is the kinematic relationship between the Geretsried Thrust and directly underlying faults with normal fault geometries?

Pre-orogenic inheritance: Did any the lower fault array develop from the pre-existing pre-orogenic faults?

370 Pre-orogenic normal faults that are oriented sub-parallel to the developing fold-and-thrust belt are the favourable structures to be extensionally reactivated during the foreland flexuring (Butler, 1989; Bry et al., 2004; Tavani et al., 2015, 2018). In the Western Molasse Basin, the basement structures are interpreted to act as the loci of the flexure-induced normal faulting (J. Mosar, personal communication, 2018). In the Eastern Molasse Basin, Budach et al. (2017) and Mraz et al. (2018) report reactivation of the Mesozoic normal faults during the Cenozoic flexuring. Based on the structural evidence, we discuss in this
375 section whether the analyzed faults of the lower fault array had a pre-orogenic activity.



The results of throw distribution on the lower faults show three major trends from top Berriasian down to top Callovian (i.e., near top basement): (i) throw diminishes (Fault NE; Fig. 15), (ii) throw decreases nearly to zero (Faults Gartenberg S and Gartenberg N; Figs. 4, 6 and 16), and (iii) throw remains constant (Fault Gelting N; Fig. 17).

The former two cases suggest that the faults propagated into the basement from the shallower stratigraphic unit. The near-
380 elliptical tip lines of faults NE and Gartenberg S imply an initially elliptical slip distribution on these faults (Barnett et al., 1987). Such slip distribution is characteristic of blind fault growth by radial propagation, whereby the site of fault nucleation typically corresponds to the region of maximum displacement (Watterson, 1986; Barnett et al., 1987; Walsch and Watterson, 1987; Baudon and Cartwright, 2008a, b). The throw distribution on the faults NE, Gartenberg S and Gartenberg N shows that the maximum displacement could occur between top Callovian and top Berriasian, suggesting that these faults nucleated within
385 the carbonate platform and were not rooted in the basement. Fault Gelting N is the only fault in our study area that could have originated within the pre-fractured basement, since it shows no decrease in displacement with depth down to top Callovian.

A substantial upward decrease in fault throw from top Berriasian to top Turonian, as is observed in the study area on faults NE (Fig. 15) and Gartenberg S (Fig. 16), has been also reported 25 km to the NNE and 55 km to the W, in the Unterhaching and Mauerstetten geothermal sites, respectively (Budach et al., 2017; Mraz et al., 2018). Such high displacement gradient can
390 indicate either (1) fault interaction with the free surface, i.e., syn-sedimentary activity, if the displacement gradient increase coincides with the stratigraphic expansion of the displaced units across faults or (2) propagation across a mechanical barrier if there is no stratigraphic expansion (Baudon and Cartwright, 2008a). The former case is confirmed in the Unterhaching and Mauerstetten areas, where, as Budach et al. (2017) and Mraz et al. (2018) infer, faults had a syn-sedimentary activity in the Mesozoic. In contrast, in this area, we do not observe stratigraphic expansion of the Turonian Unit 2 across the analysed faults.
395 Even though there is local thickening of the Turonian Unit 2 in the hanging-wall, it is accompanied by the thinning of the same unit in the footwall. This suggests ductile deformation of the Turonian sediments acted as a barrier to fault propagation. Based on this evidence, we rule out the possibility of the Mesozoic faults in the Geretsried area having attracted flexural-induced extension in the Cenozoic.

Early-orogenic inheritance: What is the kinematic relationship between the Geretsried Thrust and directly underlying 400 faults with normal fault geometries?

Early-orogenic inheritance plays a significant role in the spatial evolution of the contractional deformation. A characteristic geometrical relationship between the Geretsried Thrust and directly underlying normal faults suggests a possible kinematic interaction between them in the past. Such overprinting relationships between flexure-induced normal faults and later developed contractional structures have been recognised in foreland basins at the toe of the orogenic wedges elsewhere (e.g., Scisciani
405 et al., 2001, Bry et al., 2004, Calamita et al., 2012). According to Tavani et al. (2015), thrust fault nucleation and propagation may occur even in a strike-slip faulting stress regime, facilitated by the reverse reactivation of pre-existing normal faults that strike perpendicular to the shortening direction. These authors argue that the strain at the tips of positively inverted faults or in the overstep areas between them produces local contractional areas and causes re-orientation of the maximum principal stress axis until it reaches favourable angle with the bedding, eventually resulting in a slip. Such a local perturbation of the stress field



410 at the tips of the inverted faults may favour nucleation and propagation of an about 30° dipping, new fault segment that further
develops into a thrust fault. It is likely that the Geretsried thrust developed according to this scenario. An approximately 30°–
35° dipping thrust ramp (Fig. 13) must have initiated in the step-over area between the CZ normal faults, that were undergoing
reverse reactivation, and from there propagated both upwards and downwards. It eventually reached beneath the Upper Jurassic
carbonate platform and connected to a basal décollement beneath it. The prominent Geretsried Fold above the thrust ramp most
415 probably developed due to the buttressing of the thrust displacements against the pre-existing normal faults (e.g., Butler, 1989;
Scisciani et al., 2001).

The early-orogenic inheritance must have also influenced the style of deformation in the transition zone between the Foreland
Molasse and the Folded Molasse, immediately south of the Geretsried area. The northern extent of the Geretsried Fold within
the survey area coincides with the northern limit of the tilted Molasse on the tectonic map of the Folded Molasse by Ortner et al.
420 (2015) (Fig. 1b). The seismic profile A in Figure 10 clearly shows that the extent of the tilted Molasse south of the Geretsried
area is much narrower than shown by Ortner et al. (2015). The area of the tilted Molasse broadens significantly to the east,
while the extent of the Geretsried Thrust decreases (Fig. 11). We postulate that the varying amplitude of the tilted zone from
west to east must be controlled by the occurrence of early-orogenic normal faults that facilitate thrusting. In the Geretsried
area and south of it, the Geretsried Thrust accommodated shortening and thereby prevented large-scale folding in front of the
425 propagating Alpine thrust sheets. In contrast, to the east, in the absence of inherited extensional structures and therefore thrust
faulting, the shortening was accommodated by amplification of the tilted zone at the foot of the Kirchbichl Thrust.

6.2.3 Mechanical stratigraphy

The fault growth in the southern GMB is influenced by the different mechanical behavior of rock layers. We show in this
subsection that mechanically incompetent layers within the Meso-Cenozoic sequence act as fault propagation barriers, resulting
430 in variations in fault plane geometries, development of extensional forced folding and decoupling of the lower and upper fault
arrays.

Growth of the lower faults

As we postulated in the previous subsection, the majority of the lower faults nucleated in the carbonate platform and grew
by radial propagation. The down-dip propagation of individual faults could have been affected by the mechanical behaviour
435 of the Dogger shales/marls (below top Callovian). For instance, the occurrence of the rollover structures within the central
graben suggests that graben-bounding faults, Gartenberg S and Gartenberg N, propagated down into the detachment beneath
the carbonate platform that accommodated flexure-induced extension. Up-dip propagation was restricted by the Turonian layer
of Unit 2. We postulate that the aforementioned high displacement gradient for faults NE and Gartenberg S (Figs. 15 and 16)
resulted from the additional slip that accumulated at the mechanical boundary for the faults to propagate through the barrier
440 (e.g., Wilkins and Gross, 2002; Baudon and Cartwright, 2008a).

Two features point to a restricting behaviour of the Turonian marls: 1) extensional forced folding above tips of normal faults
and 2) the staircase geometry of Fault Gartenberg S. Mechanically incompetent layers accommodate pre-failure strain by



distributed ductile deformation, which causes extensional forced folding and thinning of the incompetent layer at the footwall (Walsch and Watterson, 1987; Withjack et al., 1990; Childs et al., 1996; Withjack and Callaway, 2000; Schöpfer et al., 2006; 445 Ferrill et al., 2012). In our study area, this kind of deformation is especially evident above the minor lower faults (Figs. 4 and 6). Here, unbreached monoclines indicate that fault propagation was arrested by the clay-rich Turonian layer, hindering the faults to interact with the free surface. Hanging-walls of the major lower faults that managed to propagate across the Turonian barrier locally exhibit normal drag, which presumably formed as precursory monoclines were breached (Fig. 6). Extensional forced folding is also confirmed by local thinning and thickening of the Turonian marls (Unit 2) across the faults (Fig. 14b).

450 The staircase geometry of Fault Gartenberg S (Fig. 6) indicates fault growth by vertical segment linkage in the presence of a mechanical barrier (Childs et al., 1996; Walsch et al., 2003; Schöpfer et al., 2006). According to the coherent fault model by Walsch et al. (2003) and discrete element models of Schöpfer et al. (2006), kinematically connected fault segments first initiate in strong layers, whereas weak layers deform by ductile flow. Increasing strain results in shear failure of the weak layers and eventual linkage of the fault segments. The resulting through-going fault thus attains a staircase geometry. The shallower 455 dip of Fault Gartenberg S within the Turonian marls corresponds to the throw minimum at top Turonian that separates two throw maxima at top Berriasian and top Priabonian (Fig. 16). We propose that ductile deformation of Unit 2 promoted vertical fault segmentation of Fault Gartenberg S, whereby an upper fault segment formed in the more competent Unit 3 and linked downwards with the lower segment of Gartenberg S within Unit 2.

460 Having considered the impact of mechanical stratigraphy, we propose the following growth history of the lower faults, which is illustrated in Figure 20:

1. Lower normal faults initiated within the carbonate platform and possibly, in case of Fault Gelting N, in the basement.
2. The faults propagated radially from the point of nucleation as blind faults. The up-dip propagation was inhibited by the Turonian marls, resulting in monoclinial folding of the overlying layers. Minor faults were arrested by the mechanical barrier, whereas major faults continued to propagate across it, in individual cases, by vertical segment linkage.
- 465 3. As fault slip continued, major faults breached the monoclines above them and reached the free surface during sedimentation of the Rupelian clays, thereby switching from being blind to syn-sedimentary. Eventually, faulting ceased and the stagnant fault tips were buried by the later Rupelian sediments.

Decoupled evolution of the fault network

As we have put forward in the previous subsection on stress field evolution, the stress conditions in the Chattian were favourable 470 for the independent development of the upper faults in the Cenozoic interval. Faults are expected to nucleate first in the most competent unit of the multi-layered Cenozoic sequence, since the less competent units are able to accommodate greater pre-failure strain (Eisenstadt and De Paor, 1987; Ferrill et al., 2017). The fault geometries suggest that the upper faults nucleated indeed within the competent Baustein beds, and grew by both up- and downward propagation. Such isolated fault growth within the Cenozoic Molasse is also reported c. 35 km E of our study area by von Hartmann et al. (2016), where the authors observe 475 decrease in throw from central to outermost portions of the Cenozoic faults, both up- and down-dip.



As the upper faults propagated downward into the incompetent Unit 4 (Rupelian), they failed to connect with the lower faults by incidental dip linkage (e.g., Baudon and Cartwright, 2008c; Langhi et al., 2011). They flattened out within the Rupelian sediments, which are expected to have a lower angle of internal friction and act as a detachment horizon (Müller et al., 1988; Ortner et al., 2015). Although the observation of fault geometry within the Rupelian sequence is limited by its semi-transparent and non-coherent reflection configuration, the listric nature of the CZ normal faults could be inferred from the thinning of Unit 4 (Rupelian) across these faults (Fig. 14d).

At the same time, it is unlikely that the lower faults accommodated Chattian deformation by reactivation and upward propagation. We do not observe monoclinical folding within the mechanically weak Rupelian strata that would have developed if the lower faults had propagated across it (Schöpfer et al., 2006). We postulate that the upward propagation of the lower faults were inhibited due to the mechanical behaviour of Rupelian clays that acted as a propagation barrier. In the latter case, the extensional strain could be accommodated by ductile, i.e., distributed, sub-seismic deformation within the Rupelian Unit 4. We conclude that the fault evolution in the presence of a thick mechanical barrier resulted in a decoupled structural style.

7 Conclusions

We used 3D seismic data from the Geretsried area to analyse the structure and evolution of the fault network proximal to the Alpine front. Structural analysis reveals that the fault network developed in three syn-orogenic deformation phases: (i) lower normal faulting in the Rupelian, (ii) upper normal faulting in the Chattian, and (iii) reverse and thrust faulting in the mid-Miocene. We demonstrate that these temporal phases correlate with the evolution of the stress field as the Alpine orogen moved forward. While the tectonic stresses are responsible for fault initiation, local stress ‘modifiers’, such as pre-existing structures and mechanical stratigraphy, govern the location of fault nucleation and its further spatial development.

A key observation of this study is that the lower and upper fault arrays developed independently, both temporally and spatially, with nucleation loci in the Upper Jurassic carbonate platform for the former fault array and in the Baustein beds for the latter. Vertical gradients of the flexural stresses pre-defined decoupled initiation of the upper faults with respect to the lower faults, whereas the mechanically incompetent Rupelian clays inhibited further geometrical connection of the two fault arrays. The decoupled style of fault evolution has implications for geothermal exploration in the GMB, since we expect the isolated lower faults to develop less interconnected fractures and be more prone to healing by secondary mineralisation than through-going faults with a prolonged activity, which are observed elsewhere in the basin. In this respect, further investigations are required to establish correlation between the decoupled faulting style and the mechanical behaviour of the Rupelian clays.

Furthermore, seismic interpretation documents kinematic interaction between the upper normal faults and large-scale thrusts. In particular, we postulate that the reactivation of CZ normal faults facilitated the initiation of the Geretsried thrust, thereby preventing a large accumulation of strain at the foot of the Folded Molasse. We therefore emphasise the importance of the early-orogenic structures on the style of contractional deformation in the transition zone between the Foreland and the Folded Molasse.



Data availability. The seismic data is not publicly accessible. The results of the seismic model are presented in the article. Detailed results can be provided by the first author on request.

510 *Author contributions.* VS designed the study, carried out the seismic interpretation and 3D structural modelling, wrote the manuscript, and prepared the figures. DT participated in analyzing the structural results and in the writing of the manuscript. HH contributed in interpreting the seismic data and drafting the manuscript. IM initiated the study. All authors commented, read, and approved the final manuscript.

Competing interests. No competing interests are present.

Acknowledgements. This work was carried out as part of the joint research project 'Play Type', financed by the German Ministry for
515 Economic Affairs and Energy (FN: 0324210A). We thank Enex Power Germany GmbH and Wintershall Dea GmbH for access to seismic and well data and permission to publish images from these data. Seismic data acquisition and processing was carried out by DMT GmbH. We also thank reviewers for their thorough reviews, which helped to improve this article. Jonas Kley, Jennifer Ziesch, Sonja Wadas, and Tom Schintgen are thanked for their useful comments on the manuscript.



References

- 520 Agemar, T., Alten, J., Ganz, B., Kuder, J., Kühne, K., Schumacher, S., and Schulz, R.: The geothermal information system for Germany — GeotIS, *Z. Dtsch. Ges. Geowiss.*, 165(2), 129–144, <https://doi.org/10.1127/1860-1804/2014/0060>, 2014.
- Allan, U. S.: Model for hydrocarbon migration and entrapment within faulted structures, *AAPG Bull.*, 73(7), 803–811, <https://doi.org/10.1306/44B4A271-170A-11D7-8645000102C1865D>, 1989.
- Allen, P. A., Crampton, S. L., and Sinclair, H. D.: The inception and early evolution of the North Alpine Foreland Basin, Switzerland, *Basin Res.*, 3(3), 143–163, <https://doi.org/10.1111/j.1365-2117.1991.tb00124.x>, 1991.
- 525 Bachmann, G. H., Dohr, G., and Müller, M.: Exploration in a classic thrust belt and its foreland, Bavarian Alps, Germany, *AAPG Bull.*, 66(12), 2529–2542, <https://doi.org/10.1306/03B5AC69-16D1-11D7-8645000102C1865D>, 1982.
- Bachmann, G. H., Müller, M., and Weggen, K.: Evolution of the Molasse Basin (Germany, Switzerland), *Tectonophysics*, 137, 77–92, [https://doi.org/10.1016/0040-1951\(87\)90315-5](https://doi.org/10.1016/0040-1951(87)90315-5), 1987.
- 530 Bachmann, G. H., and Müller, M.: The Molasse Basin, Germany: evolution of a classic petroliferous foreland basin, in: *Generation, Accumulation and Production of Europe's Hydrocarbons*, edited by: Spencer, A. M. et al., *Spec. Publ. Eur. Assoc. Petrol. Geosci.*, No. 1, 263–276, 1991.
- Bachmann, G. H., and Müller, M.: Sedimentary and structural evolution of the German Molasse Basin, *Ecolae Geol. Helv.*, 85(3), 519–530, 1992.
- 535 Barnett, J. A. M., Mortimer, J., Rippon, J. H., Walsh, J. J. and Watterson, J.: Displacement geometry in the volume containing a single normal fault, *AAPG Bull.*, 71(8), 925–937, <https://doi.org/10.1306/948878ED-1704-11D7-8645000102C1865D>, 1987.
- Baudon, C., and Cartwright, J. A.: 3D seismic characterisation of an array of blind normal faults in the Levant Basin, Eastern Mediterranean, *Journal of Structural Geology*, 30, 746–760, <https://doi.org/10.1016/j.jsg.2007.12.008>, 2008a.
- Baudon, C., and Cartwright, J.: Early stage evolution of growth faults: 3D seismic insights from the Levant Basin, Eastern Mediterranean, *Journal of Structural Geology*, 30, 888–898, <https://doi.org/10.1016/j.jsg.2008.02.019>, 2008b.
- 540 Baudon, C., and Cartwright, J.: The kinematics of reactivation of normal faults using high resolution throw mapping, *Journal of Structural Geology*, 30, 1072–1084, <https://doi.org/10.1016/j.jsg.2008.04.008>, 2008c.
- Bradley, D. C., and Kidd, W. S. F.: Flexural extension of the upper continental crust in collisional foredeeps, *Bull. Geol. Soc. Am.*, 103, 1416–1438, [https://doi.org/10.1130/0016-7606\(1991\)103<1416:FEOTUC>2.3.CO;2](https://doi.org/10.1130/0016-7606(1991)103<1416:FEOTUC>2.3.CO;2), 1991.
- 545 Bry, M., White, N., Singh, S., England, R., and Trowell, C.: Anatomy and formation of oblique continental collision: South Falkland basin, *Tectonics*, 23, TC4011, <https://doi.org/10.1029/2002TC001482>, 2004.
- Budach, I., Moeck, I., Lüschen, E., and Wolfgramm, M.: Temporal evolution of fault systems in the Upper Jurassic of the Central German Molasse Basin: case study Unterhaching, *Int. J. Earth Sci. (Geol. Rundsch.)*, 107, 635–654, <https://doi.org/10.1007/s00531-017-1518-1>, 2017.
- 550 Butler, R. W. H.: The influence of pre-existing basin structure on thrust system evolution in the Western Alps, *Geological Society, London, Special Publications*, 44, 105–122, <https://doi.org/10.1144/GSL.SP.1989.044.01.07>, 1989.
- Cartwright, J. A., Bourouillec, R., James, D., and Johnson, H. D.: Polycyclic motion history of some Gulf Coast growth faults from high-resolution displacement analysis, *Geology*, 26(9), 819–822, [https://doi.org/10.1130/0091-7613\(1998\)026<0819:PMHOSG>2.3.CO;2](https://doi.org/10.1130/0091-7613(1998)026<0819:PMHOSG>2.3.CO;2), 1998.



- 555 Calamita, F., Pace, P., and Satolli, S.: Coexistence of fault-propagation and fault-bend folding in curve-shaped foreland fold-and-thrust belts: Examples from the Northern Apennines (Italy), *Terra Nova*, 24, 396–406, <https://doi.org/10.1111/j.1365-3121.2012.01079.x>, 2012.
- Childs, C., Nicol, A., Walsh, J. J., and Watterson, J.: Growth of vertically segmented normal faults, *J. Struct. Geol.*, 18(12), 1389–1397, [https://doi.org/10.1016/S0191-8141\(96\)00060-0](https://doi.org/10.1016/S0191-8141(96)00060-0), 1996.
- DeCelles, P. G. and Giles, K. A.: Foreland basin systems, *Basin Res.*, 8, 105–123, <https://doi.org/10.1046/j.1365-2117.1996.01491.x>, 1996.
- 560 Diem, B.: Die Untere Meeresmolasse zwischen Saane (Westschweiz) und der Ammer (Oberbayern), *Ecl. Geol. Helv.*, 79, 493–559, 1986.
- Drews, M. C., Bauer, W., Caracciolo, L., and Stollhofen H.: Disequilibrium compaction overpressure in shales of the Bavarian Foreland Molasse Basin: Results and geographical distribution from velocity-based analyses, *Marine and Petroleum Geology*, 24, 37–50, <https://doi.org/10.1016/j.marpetgeo.2018.02.017>, 2018.
- Eisenstadt, E., and De Paor, D. G.: Alternative model of thrust-fault propagation, *Geology*, 15(7), 630–633, [https://doi.org/10.1130/0091-7613\(1987\)15<630:AMOTP>2.0.CO;2](https://doi.org/10.1130/0091-7613(1987)15<630:AMOTP>2.0.CO;2), 1987.
- 565 Ferrill, D. A., Morris, A. P., and McGinnis, R. N.: Extensional fault-propagation folding in mechanically layered rocks: The case against the frictional drag mechanism, *Tectonophysics*, 576–577, 78–85, <https://doi.org/10.1016/j.tecto.2012.05.023>, 2012.
- Ferrill, D. A., Morris, A. P., McGinnis, R. N., Smart, K. J., Wigginton, S. S., and Hill, N. J.: Mechanical stratigraphy and normal faulting, *Journal of Structural Geology*, 94, 275–302, <https://doi.org/10.1016/j.jsg.2016.11.010>, 2017.
- 570 Fischer, W.: Stratigraphische und tektonische Beobachtungen im Gebiet der Mumauer Mulde und Steineberg Mulde (Oberbayern, Allgäu und Vorarlberg), *Bull. Ver. Schweiz. Petrol.-Geol. u.-Ing.*, 27, 39–57, 1960.
- Frisch, W.: Tectonic progradation and plate tectonic evolution of the Alps, *Tectonophysics*, 69, 121–139, [https://doi.org/10.1016/0040-1951\(79\)90155-0](https://doi.org/10.1016/0040-1951(79)90155-0), 1979.
- GeoMol Team: GeoMol — Assessing subsurface potentials of the Alpine Foreland Basins for sustainable planning and use of natural resources, Project Report, LfU, Augsburg, 188 pp., 2005.
- 575 Jackson, C. A.-L., and Larsen, E.: Temporal and spatial development of a gravity-driven normal fault array: Middle–Upper Jurassic, South Viking Graben, northern North Sea, *Journal of Structural Geology*, 31, 388–402, <https://doi.org/10.1016/j.jsg.2009.01.007>, 2009.
- Jackson, C. A.-L., and Rotevatn, A.: 3D seismic analysis of the structure and evolution of a salt-influenced normal fault zone: a test of competing fault growth models. *Journal of Structural Geology*, 54, 215–234, <https://doi.org/10.1016/j.jsg.2013.06.012>, 2013.
- 580 Jin, J., Aigner, T., Luterbacher, H. P., Bachmann, G. H., and Müller, M.: Sequence stratigraphy and depositional history in the south-eastern German Molasse Basin, *Mar. Pet. Geol.*, 12, 929–940, [https://doi.org/10.1016/0264-8172\(95\)98856-Z](https://doi.org/10.1016/0264-8172(95)98856-Z), 1995.
- Kley, J., and Voigt, T.: Late Cretaceous intraplate thrusting in central Europe: Effect of Africa-Iberia-Europe convergence, not Alpine collision, *Geology*, 36(11), 839–842, <https://doi.org/10.1130/G24930A.1>, 2015.
- Kuhlemann, J., and Kempf, O.: Post-Eocene evolution of the North Alpine Foreland Basin and its response Alpine tectonics, *Sedimentary Geology*, 152, 45–78, [https://doi.org/10.1016/S0037-0738\(01\)00285-8](https://doi.org/10.1016/S0037-0738(01)00285-8), 2002.
- 585 Langhi, L., Ciftci, N. B., and Borel, G. D.: Impact of lithospheric flexure on the evolution of shallow faults in the Timor foreland system, *Marine Geology*, 284, 40–54, <https://doi.org/10.1016/j.margeo.2011.03.007>, 2011.
- Lemcke, K.: Zur nachpermischen Geschichte des nördlichen Alpenvorlandes, *Geologica Bavarica*, 69, 5–48, 1973.
- Lemcke, K.: Geologie von Bayern, Bd. 1, Das bayerische Alpenvorland vor der Eiszeit, E. Schweizerbart'sche Verlagsbuchhandlung, 590 Stuttgart, 1988.



- Londoño, J., and Lorenzo, J. M.: Geodynamics of continental plate collision during late tertiary foreland basin evolution in the Timor Sea: constraints from foreland sequences, elastic flexure and normal faulting, *Tectonophysics*, 392, 37–54, <https://doi.org/10.1016/j.tecto.2004.04.007>, 2004.
- Lüschen, E., Borrini, D., Gebrande, H., Lammerer, B., Millahn, K., Neubauer, F., and Nicolich, R.: TRANSALP — deep crustal Vibroseis and explosive seismic profiling in the Eastern Alps, *Tectonophysics*, 414(1–4), 9–38, <https://doi.org/10.1016/j.tecto.2005.10.014>, 2006.
- Lüschen, E., Dussel, M., Thomas, R., and Schulz, R.: 3D seismic survey for geothermal exploration at Unterhaching, Munich, Germany, *First Break*, 29(1), 45–54, <https://doi.org/10.3997/1365-2397.2011002>, 2011.
- Mallet, J.-L.: *Geomodeling*. Applied Geostatistics Series, Oxford University Press, New York, USA, 612 pp., 2002.
- Marfurt, K. J.: Chapter 2, Seismic Attributes and What They Measure, in: *Distinguished Instructor Series: Seismic Attributes as the Framework for Data Integration Throughout the Oilfield Life Cycle*. SEG Books, 25–150, <https://doi.org/10.1190/1.9781560803522.ch2>, 2018.
- Meyer, R. K. F., and Schmidt-Kaler, H.: *Paläogeographischer Atlas des Süddeutschen Oberjura (Malm)*, E. Schweizerbart'sche Verlagsbuchhandlung, Stuttgart, 1990.
- Moeck, I.: Catalog of geothermal play types based on geologic controls, *Renewable and Sustainable Energy Reviews*, 37, 867–882, <https://doi.org/10.1016/j.rser.2014.05.032>, 2014.
- Mraz, E., Moeck, I., Bissman, S., and Hild, S.: Multiphase fossil normal faults as geothermal exploration targets in the Western Bavarian Molasse Basin: Case study Mauerstetten, *Z. Dt. Ges. Geowiss.*, 169(3), 389–411, <https://doi.org/10.1127/zdgg/2018/0166>, 2018.
- Müller, M.: Das Ergebnis der Bohrung Staffelsee 1 als Grundlage für neue Vorstellungen über Bau und Untergrund der gefalteten Molasse, *Geologica Bavarica*, 63, 86–106, 1970.
- Müller, M., Nieberding, F., and Wanninger, A.: Tectonic style and pressure distribution at the northern margin of the Alps between Lake Constance and the River Inn, *Geol. Rundsch.*, 77(3), 787–796, <https://doi.org/10.1007/BF01830185>, 1988.
- Müller, M., and Nieberding, F.: Principles of abnormal pressures related to tectonic developments and their implication for drilling activities (Bavarian Alps, Germany), in: *Oil and Gas in Alpidic Thrustbelts and Basins of Central and Eastern Europe*, edited by: Wessely, G., and Liebl, W., EAGE Spec. Pub., 119–126, 1996.
- Ortner, H., Aichholzer, S., Zerlauth, M., Pilser, R., and Fügenschuh, B.: Geometry, amount, and sequence of thrusting in the Subalpine Molasse of western Austria and southern Germany, *European Alps, Tectonics*, 34, 1–30, <https://doi.org/10.1002/2014TC003550>, 2015.
- Paradigm Ltd.: *SKUA-GOCAD*, 2017.
- Pfiffner, O. A.: Tectonic evolution of Europe — Alpine Orogeny, in: *A Continent Revealed: The European Geotraverse*, edited by: Blundell, D., Freeman, R., and Mueller, S., University Press Cambridge, Cambridge, U.K., 180–190, <https://doi.org/10.1017/CBO9780511608261>, 1992.
- Price, N. J. and Cosgrove, J. W.: *Analysis of geological structures*, Cambridge University Press, Cambridge, 502 pp., 1990.
- Reinecker, J., Tingay, M., Müller, B., and Heidbach, O.: Present-day stress orientation in the Molasse Basin, *Tectonophysics*, 482, 129–138, <https://doi.org/10.1016/j.tecto.2009.07.021>, 2010.
- Schöpfer, M. P. J., Childs, C., and Walsh, J. J.: Location of normal faults in multilayer sequences, *Journal of Structural Geology*, 28, 816–833, <https://doi.org/10.1016/j.jsg.2006.02.003>, 2006.
- Schulz, R., Thomas, R., Jung, R., and Schellschmidt, R.: Geoscientific prospect evaluation for the Unterhaching geothermal power plant, *Z. Angew. Geol.*, 50(2), 28–36, 2004.
- Scisciani, V., Tavarnelli, E., and Calamita, F.: Styles of tectonic inversion within syn-orogenic basins: examples from the Central Apennines, Italy, *Terra Nova*, 13, 321–326, <https://doi.org/10.1046/j.1365-3121.2001.00352.x>, 2001.



- Sissingh, W.: Tectonostratigraphy of the North Alpine Foreland Basin: correlation of Tertiary depositional cycles and orogenic phases, *Tectonophysics*, 282, 223–256, [https://doi.org/10.1016/S0040-1951\(97\)00221-7](https://doi.org/10.1016/S0040-1951(97)00221-7), 1997.
- 630 Tavani, S., Storti, F., Lacombe, O., Corradetti, A., Muñoz, J. A., and Mazzoli, S.: A review of deformation pattern templates in foreland basin systems and fold-and-thrust belts: Implications for the state of stress in the frontal regions of thrust wedges, *Earth-Science Reviews*, 141, 82–104, <https://doi.org/10.1016/j.earscirev.2014.11.013>, 2015.
- Tavani, S., Corradetti, A., Sabbatino, M., Morsalnejad, D., and Mazzoli, S.: The Meso-Cenozoic fracture pattern of the Lurestan region, Iran: The role of rifting, convergence, and differential compaction in the development of pre-orogenic oblique fractures in the Zagros Belt, *Tectonophysics*, 749, 104–119, <https://doi.org/10.1016/j.tecto.2018.10.031>, 2018.
- 635 Tavarnelli E., and Peacock D. C. P.: From extension to contraction in syn-orogenic foredeep basins: the Contessa section, Umbria-Marche Apennines, Italy, *Terra Nova*, 11, 55–60, <https://doi.org/10.1046/j.1365-3121.1999.00225.x>, 1999.
- Turcotte, D. L., and Schubert, G.: *Geodynamics*, J. Wiley and Sons, New York, 1982.
- 640 Tvedt, A. B. M., Rotevatn, A., Jackson, C. A.-L., Fossen, H., and Gawthorpe, R. L.: Growth of normal faults in multilayer sequences: A 3D seismic case study from the Egersund Basin, Norwegian North Sea, *Journal of Structural Geology*, 55, 1–20, <https://doi.org/10.1016/j.jsg.2013.08.002>, 2013.
- Unger, H. J.: Die Lithozonen der Oberen Süßwassermolasse Südostbayerns und ihre vermutlichen zeitlichen Äquivalente gegen Westen und Osten, *Geol. Bav.*, 94, 19–237, 1989.
- 645 von Guembel, C. W.: Geognostische Beschreibung des bayerischen Alpengebirges und seines Vorlandes, *J. Perthes*, 1, 1–440, 1861.
- von Hagke, C., Lujendjik, E., Ondrak, R., and Lindow, J.: Quantifying erosion rates in the Molasse basin using a high resolution data set and a new thermal model, *Geotect. Res.*, 97, 94–97, <https://doi.org/10.1127/1864-5658/2015-36>, 2015.
- von Hartmann, H., Tanner, D. C., and Schumacher, S.: Initiation and development of normal faults within the German alpine foreland basin: The inconspicuous role of basement structures, *AGU Tectonics*, 35, 1560–1574, <https://doi.org/10.1002/2016TC004176>, 2016.
- 650 Walsh, J. J., and Watterson, J.: Distributions of cumulative displacement and seismic slip on a single normal fault surface, *Journal of Structural Geology*, 9(8), 1039–1046, [https://doi.org/10.1016/0191-8141\(87\)90012-5](https://doi.org/10.1016/0191-8141(87)90012-5), 1987.
- Walsh, J. J., Bailey, W. R., Childs, C., Nicol, A., and Bonson, C. G.: Formation of segmented normal faults: A 3-D perspective, *Journal of Structural Geology*, 25, 1251–1262, [https://doi.org/10.1016/S0191-8141\(02\)00161-X](https://doi.org/10.1016/S0191-8141(02)00161-X), 2003.
- Watterson, J.: Fault dimensions, displacements and growth, *Pure and Applied Geophysics*, 124, 365–373, <https://doi.org/10.1007/BF00875732>, 1986.
- 655 Weides, S., and Majorowicz, J.: Implications of spatial variability in heat flow for geothermal resource evaluation in large foreland basins: the case of the Western Canada Sedimentary Basin, *Energies*, 7(4), 2573–2594, <https://doi.org/10.3390/en7042573>, 2014.
- Wibberley, C. A. J., Kurz, W., Imber, J., Holdsworth, R. E., and Colletini, C. (eds.): *The Internal Structure of Fault Zones: Implications for Mechanical and Fluid-Flow Properties*, *Geol Soc. London Sp. Publ.*, 299, 2008.
- 660 Wilkins, S. J., and Gross, M. R.: Normal fault growth in layered rocks at Split Mountain, Utah: influence of mechanical stratigraphy on dip linkage, fault restriction and fault scaling, *Journal of Structural Geology*, 24(9), 1413–1429, [https://doi.org/10.1016/S0191-8141\(01\)00154-7](https://doi.org/10.1016/S0191-8141(01)00154-7), 2002.
- Withjack, M. O., Olson, J. E., and Peterson, E.: Experimental models of extensional forced folds, *AAPG Bull.*, 74, 1038–1054, <https://doi.org/10.1306/0C9B23FD-1710-11D7-8645000102C1865D>, 1990.
- 665 Withjack, M. O., and Callaway, S.: Active normal faulting beneath a salt layer: an experimental study of deformation patterns in the cover sequence, *AAPG Bull.*, 84(5), 627–651, <https://doi.org/10.1306/C9EBCE73-1735-11D7-8645000102C1865D>, 2000.



- Ziegler, P. A.: Geological Atlas of Western and Central Europe, Shell Internationale Petroleum Maatschappij, B.V., The Hague, 1990.
- Ziegler, P. A., Cloetingh, S., and van Wees, J.-D.: Dynamics of intra-plate compressional deformation: the Alpine foreland and other examples, *Tectonophysics*, 252, 7–59, [https://doi.org/10.1016/0040-1951\(95\)00102-6](https://doi.org/10.1016/0040-1951(95)00102-6), 1995.
- 670 Ziesch, J., Aruffo, C. M., Tanner, D. C., Beilecke, T., Dance, T., Henk, A., Weber, B., Tenthorey, E., Lippmann, A., and Krawczyk, C. M.: Geological structure of the CO2CRC Otway Project site, Australia: Fault kinematics based on quantitative 3D seismic interpretation, *Basin Research*, 29(2), 129–148, <https://doi.org/10.1111/bre.12146>, 2017.
- Zweigel, J.: Eustatic versus tectonic control on foreland basin fill. Sequence stratigraphy, subsidence analysis, stratigraphic modelling, and reservoir modelling applied to the German Molasse Basin, *Contr. Sedimen. Geol*, Stuttgart: E. Schweizerbart'sche Verlagsbuchhandlung, 675 1998.

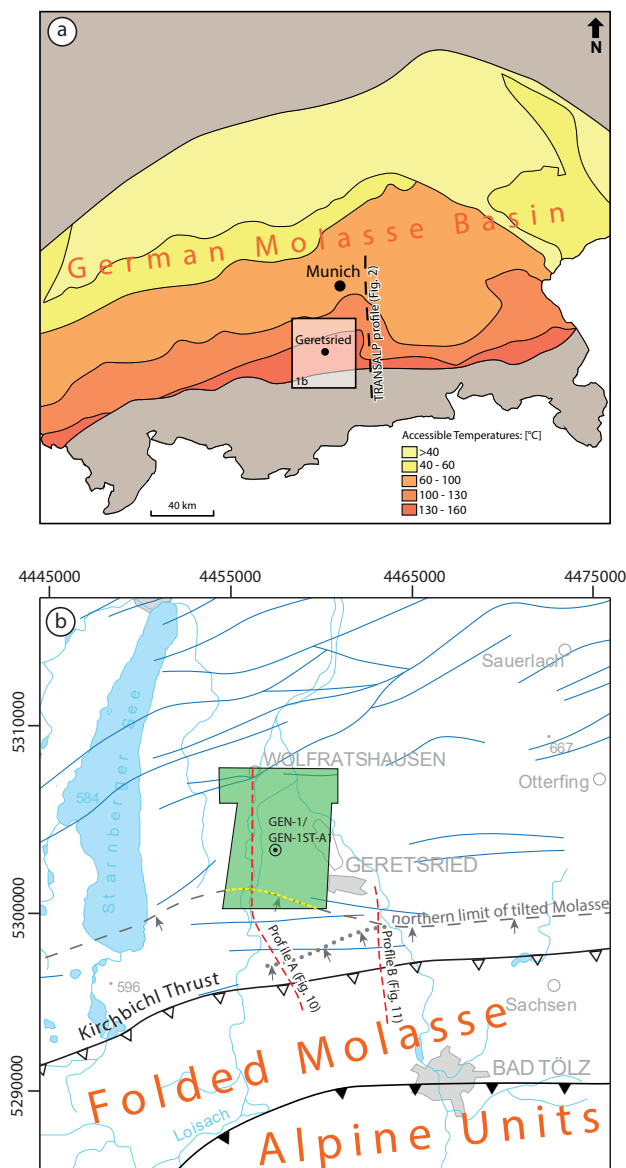


Figure 1. Location map. (a) Outline of the German Molasse Basin with geothermal areas (Agemar et al., 1914). Black dashed line shows the location of the regional cross-section in Figure 2. Black box marks area shown in b. (b) Close-up of the study area, showing the extent of the 3D seismic survey, the location of two seismic profiles and well GEN-1. Blue lines are traces of major normal faults in the Upper Jurassic carbonate platform (GeoMol Team, 2005). The dashed yellow line shows the N extent of the Geretsried Fold. The dashed grey line marks the N limit of the tilted Molasse according to the tectonic map of the Folded Molasse by Ortner et al. (2015), whereas the dotted line is the interpretation of the N limit of the Folded Molasse based on this study.

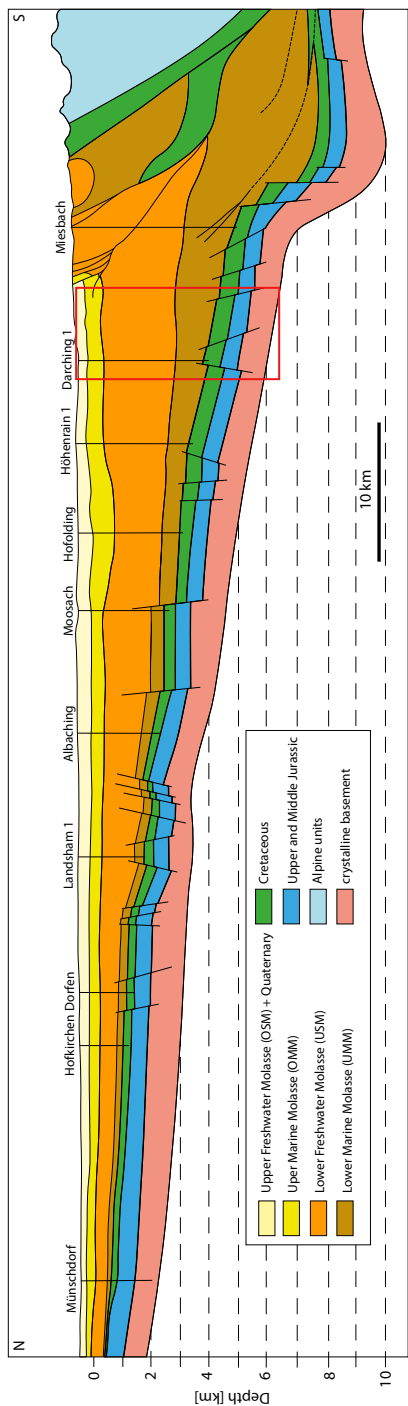


Figure 2. Simplified cross-section across the Molasse Basin, based on the interpretation of the seismic TRANSALP profile (after Lüschen et al., 2006), located 30 km to the east of the study area. For location, see Fig. 1a. The red box marks the projection of the study area.

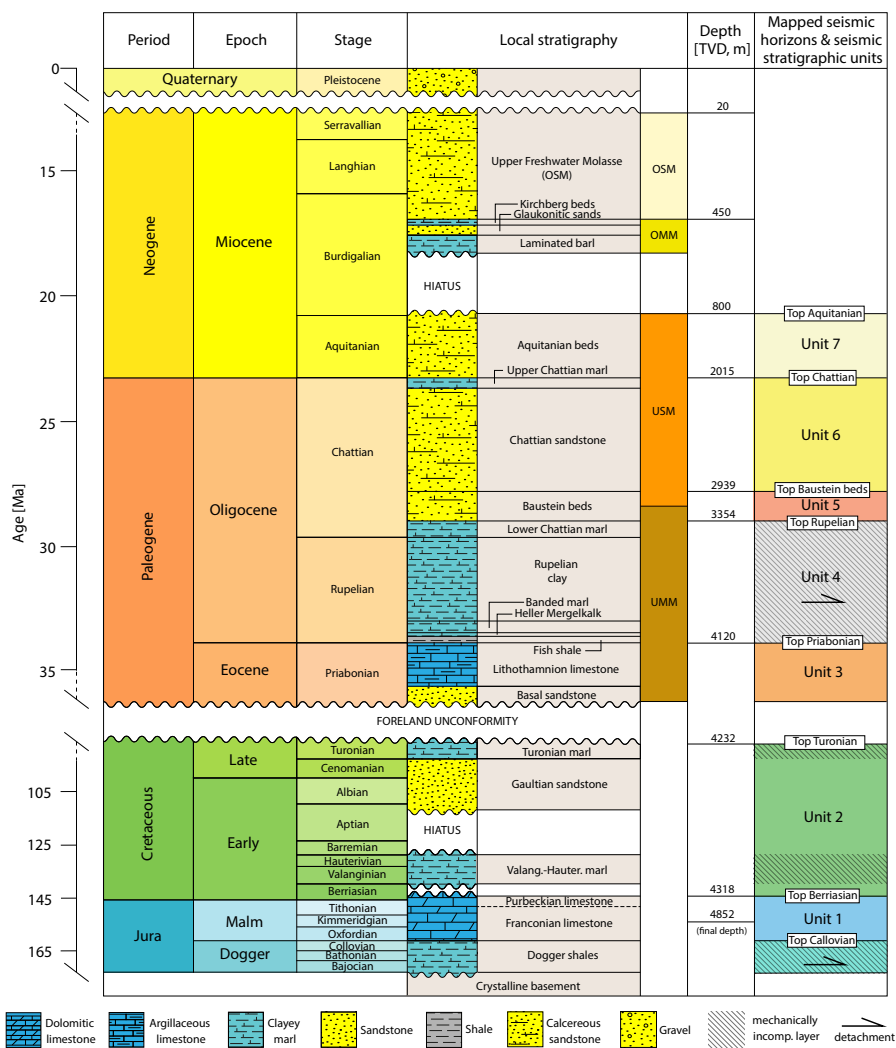


Figure 3. Detailed stratigraphy of the study area. Formation tops in depth were taken from the GEN-1 well. Qualitative mechanical stratigraphy (Fischer, 1960; Müller, 1970; Budach et al., 2017) and the location of inferred detachments (Bachmann et al., 1982; Müller et al., 1988; Ortner et al., 2015; von Hartmann et al., 2016) are also indicated. Mapped seismic horizons, and the stratal units they bound, are depicted in the right column. For stratigraphic abbreviations see Fig. 2.

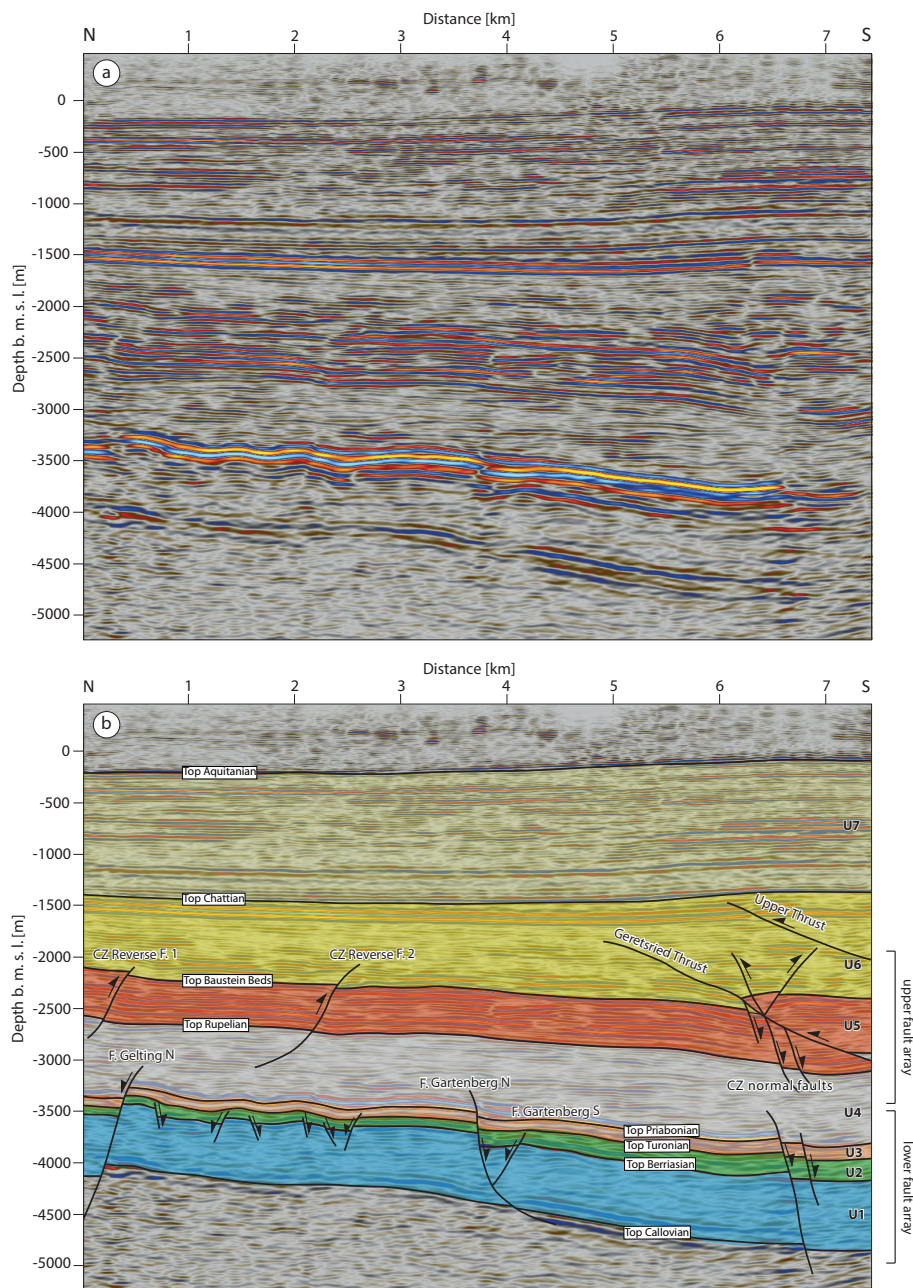


Figure 4. N—S-oriented seismic section across the centre of the 3D survey (see Fig. 8 for location). (a) Depth section. (b) Geoseismic section with interpreted seismic-stratigraphic units and faults, which illustrates that lower faults and upper faults are geometrically decoupled. The faults we refer to in this work are named.

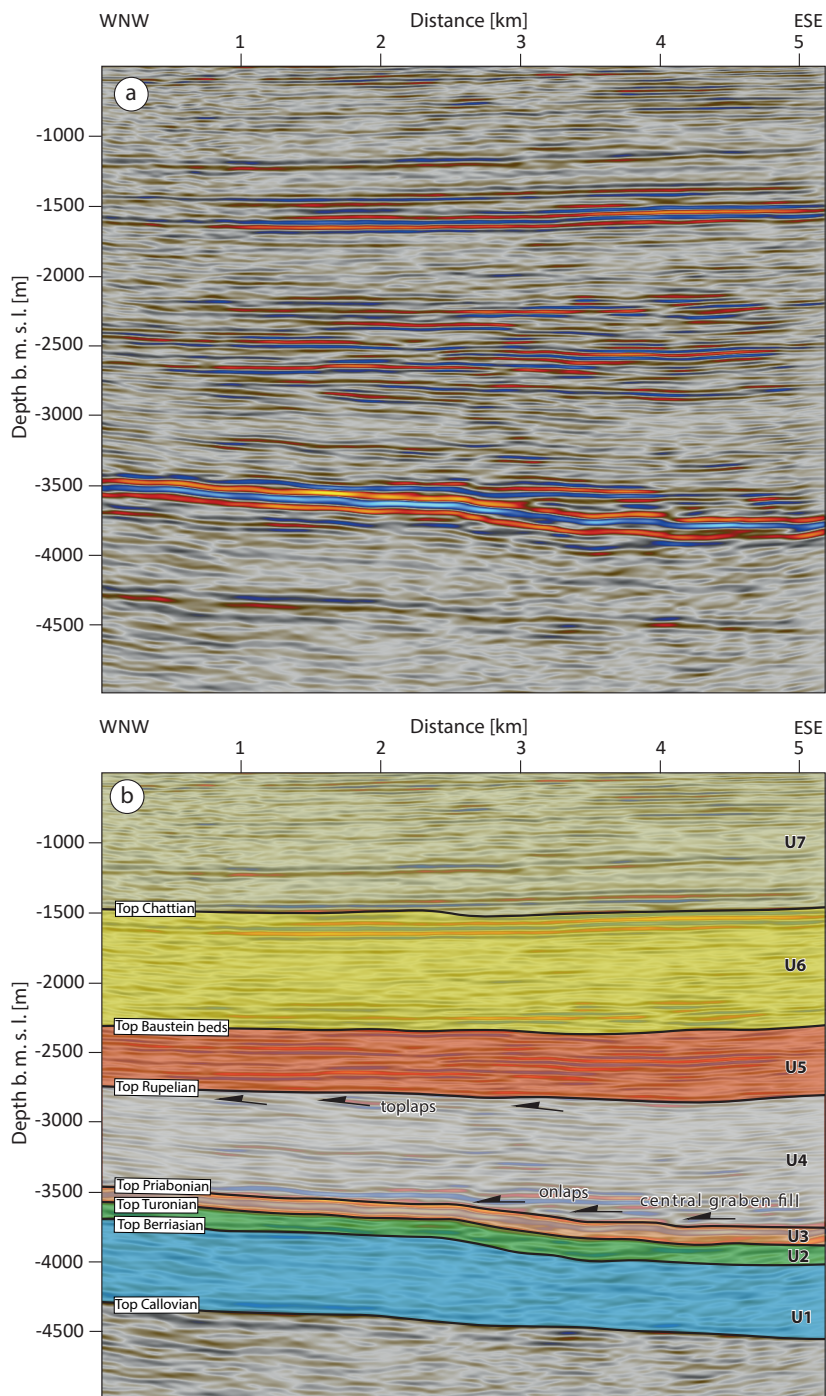


Figure 5. WNW–ESE-oriented seismic section (a) with interpretation (b) through the central graben, along its strike (see Fig. 8a for location). It shows thinning of Unit 1 (carbonate platform), onlapping and toplapping of reflections within Unit 4.

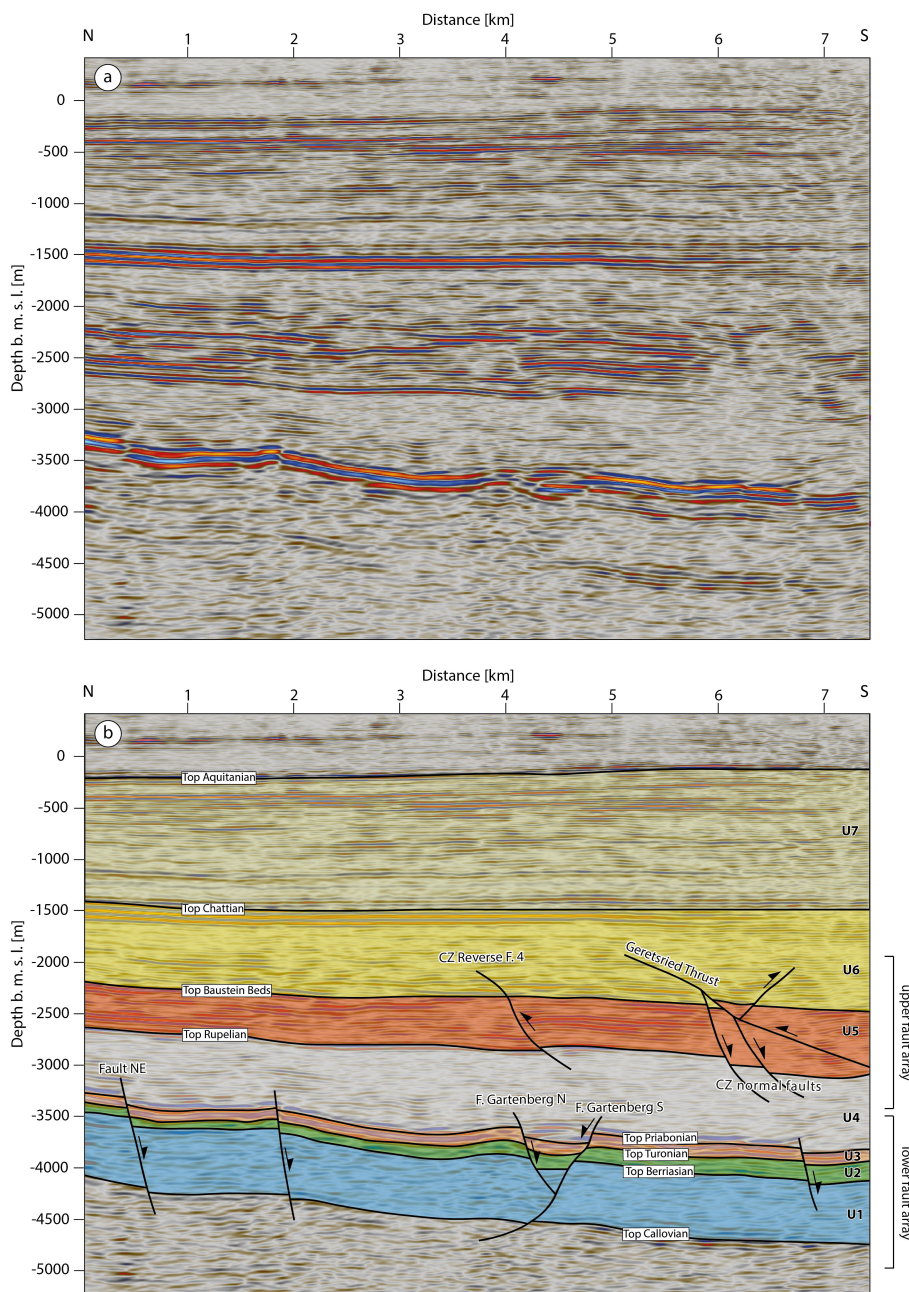


Figure 6. N–S-oriented seismic section across the eastern margin of the 3D survey (see Fig. 8 for location). (a) Depth section. (b) Geoseismic section with interpreted seismic-stratigraphic units and faults. The faults we refer to in this work are named.

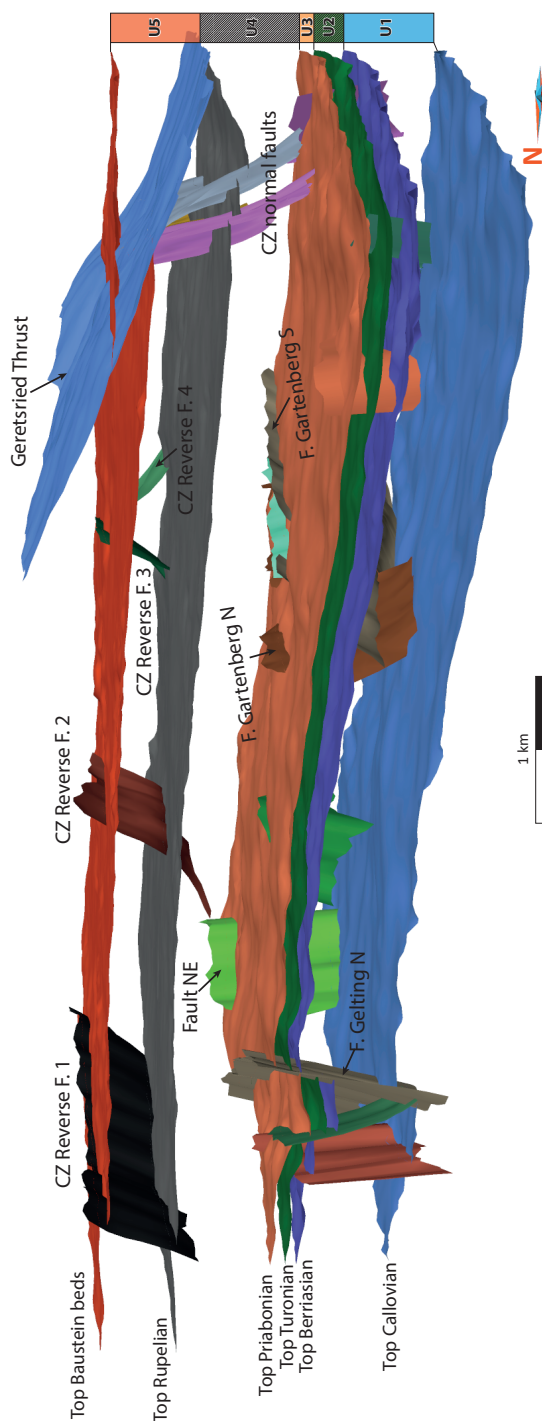


Figure 7. Oblique, WSW view of the 3D structural model showing two distinct fault arrays. The faults we refer to in this work are named.

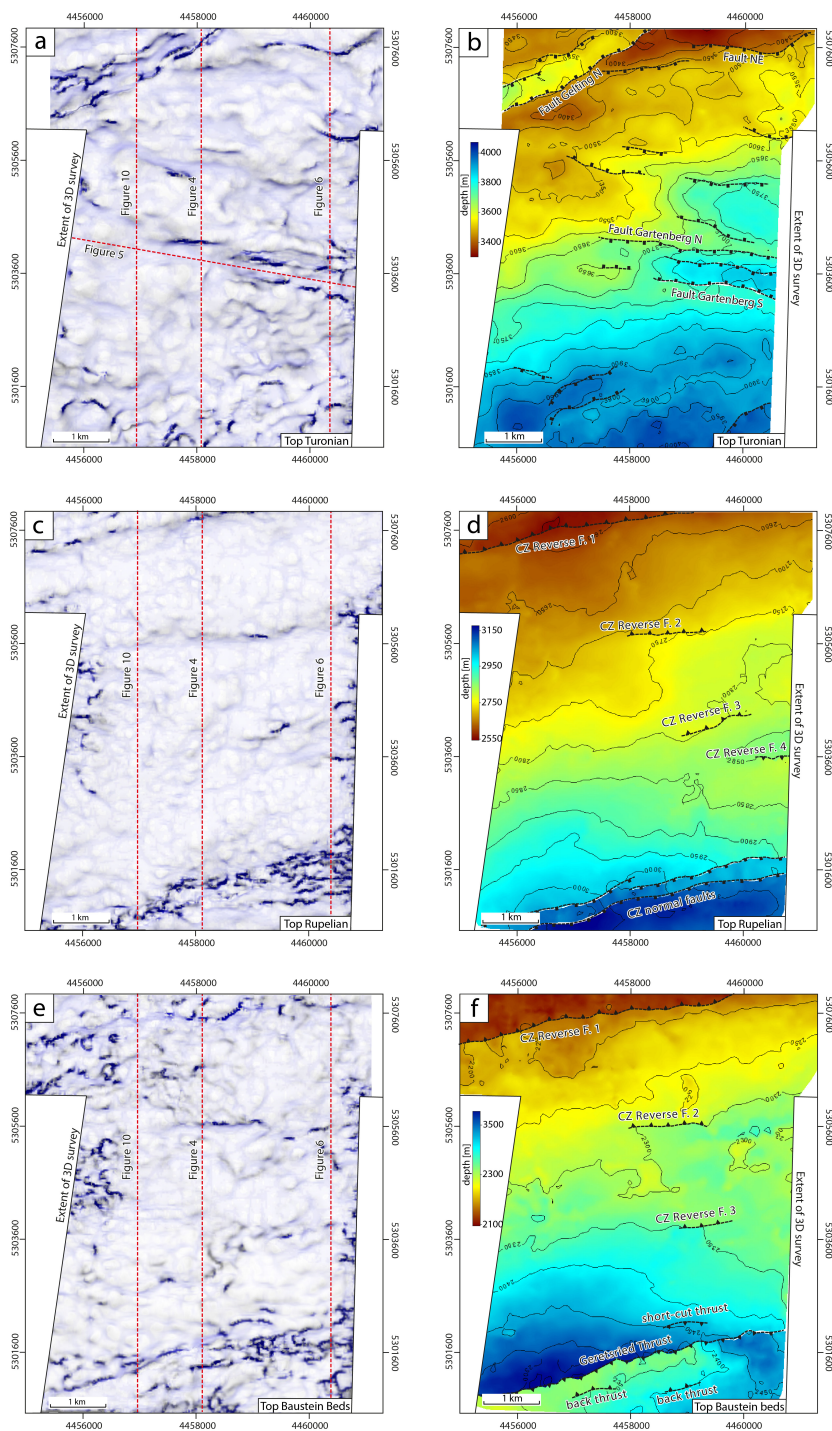


Figure 8. Co-rendered variance and most negative curvature multiattribute maps and depth-structure maps, showing: (a, b) lower fault array at top Turonian, and (c, d) upper fault array at Top Rupelian and (e, f) at top Baustein beds.

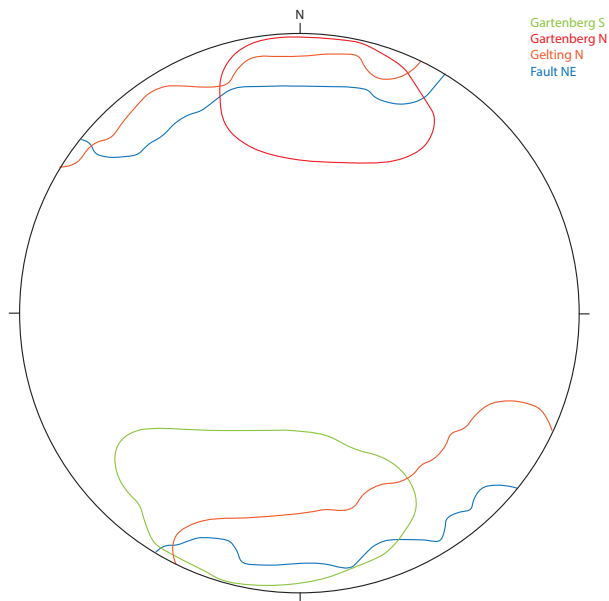


Figure 9. Isolines of the densities (> 1%) of the uniform distribution of poles to triangles that make up the surfaces of the lower faults, colour coded by fault. Lower hemisphere projection.

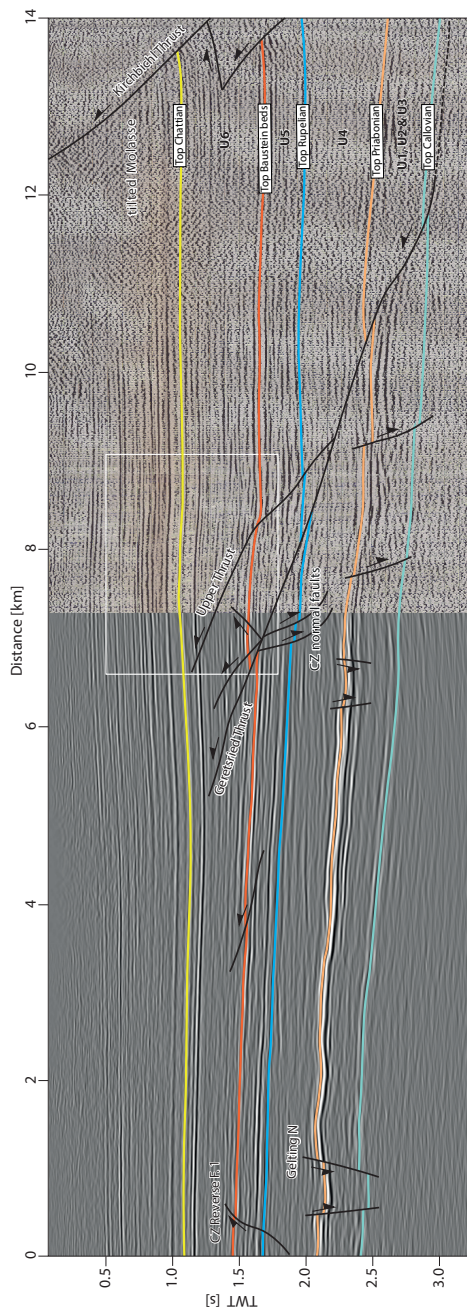


Figure 10. N–S oriented seismic time profile A across the study area to the frontal thrust (i.e., Kirchbichl Thrust) of the Folded Molasse. It was produced by merging a cross-section from the 3D Geretsried seismic survey (left) and a 2D seismic line acquired in 1987 (right). The profile shows the extent and the cross-sectional geometry of the two major thrusts. The white box marks thrust-related folding within the hanging-wall of the Geretsried Thrust. For location, see Fig. 1b.

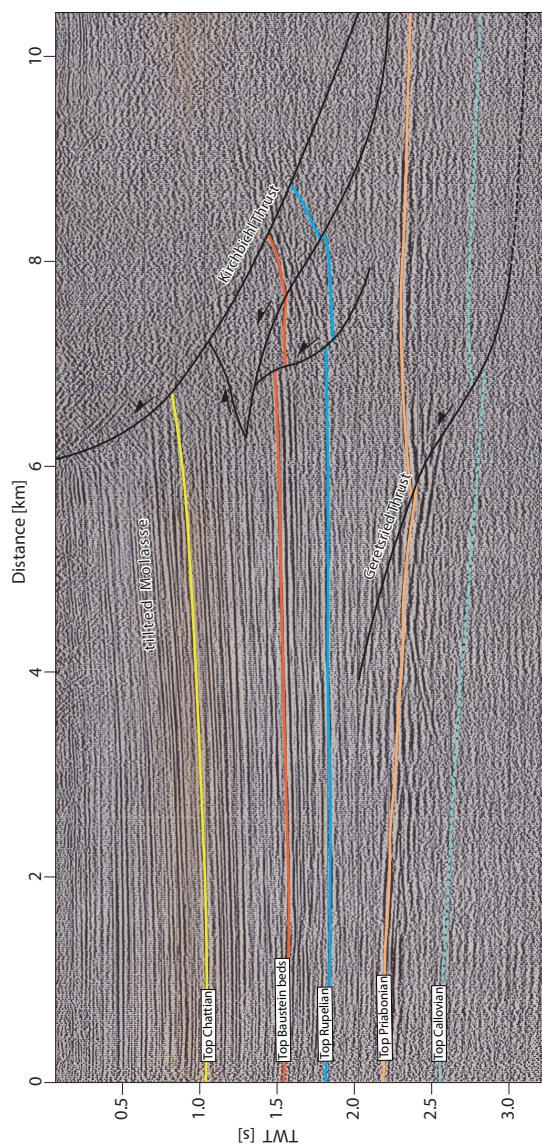


Figure 11. N–S oriented seismic time profile B, c. 3–5 km southeast of the Geretsried survey area. Note that the zone of tilted Molasse is much broader at this location. For location see Figure 1b.

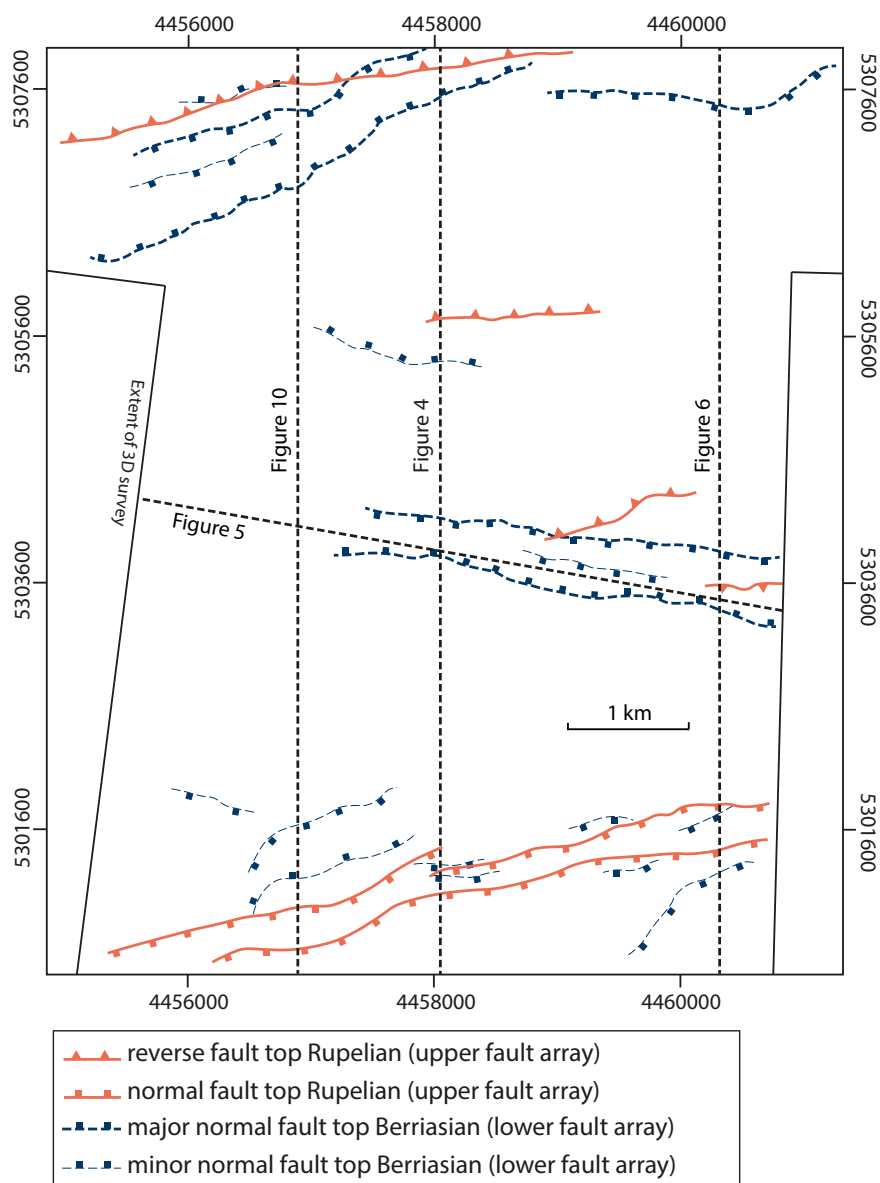


Figure 12. Map of fault traces interpreted within the 3D seismic volume. Blue dashed lines are major and minor lower faults at top Berriasian, orange solid lines are upper faults at top Rupelian. The locations of the three cross-sections shown in Figures 4–6 and 10 are shown.

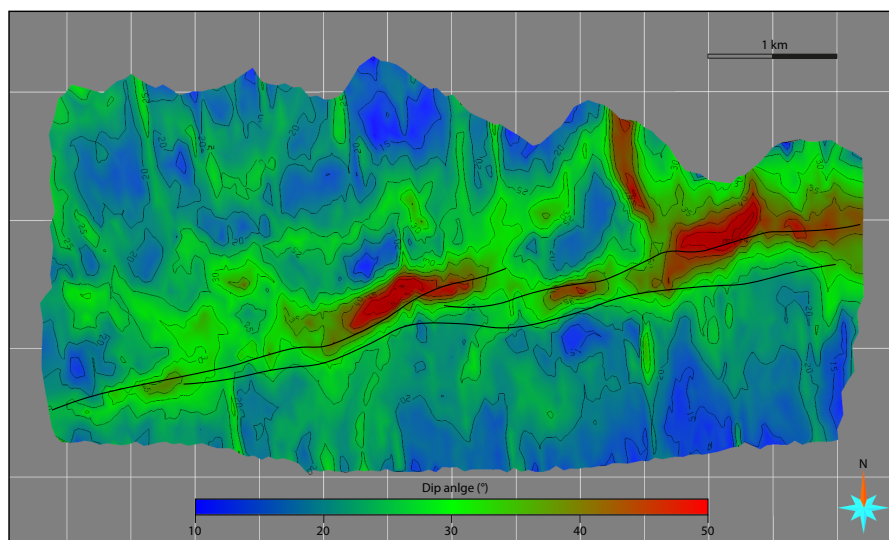


Figure 13. Dip angle distribution on the Geretsried Thrust (map view). The black lines represent traces of the CZ normal faults juxtaposed by the Geretsried Thrust. Note that the step-over region between the CZ normal faults is characterised by higher dip angle.

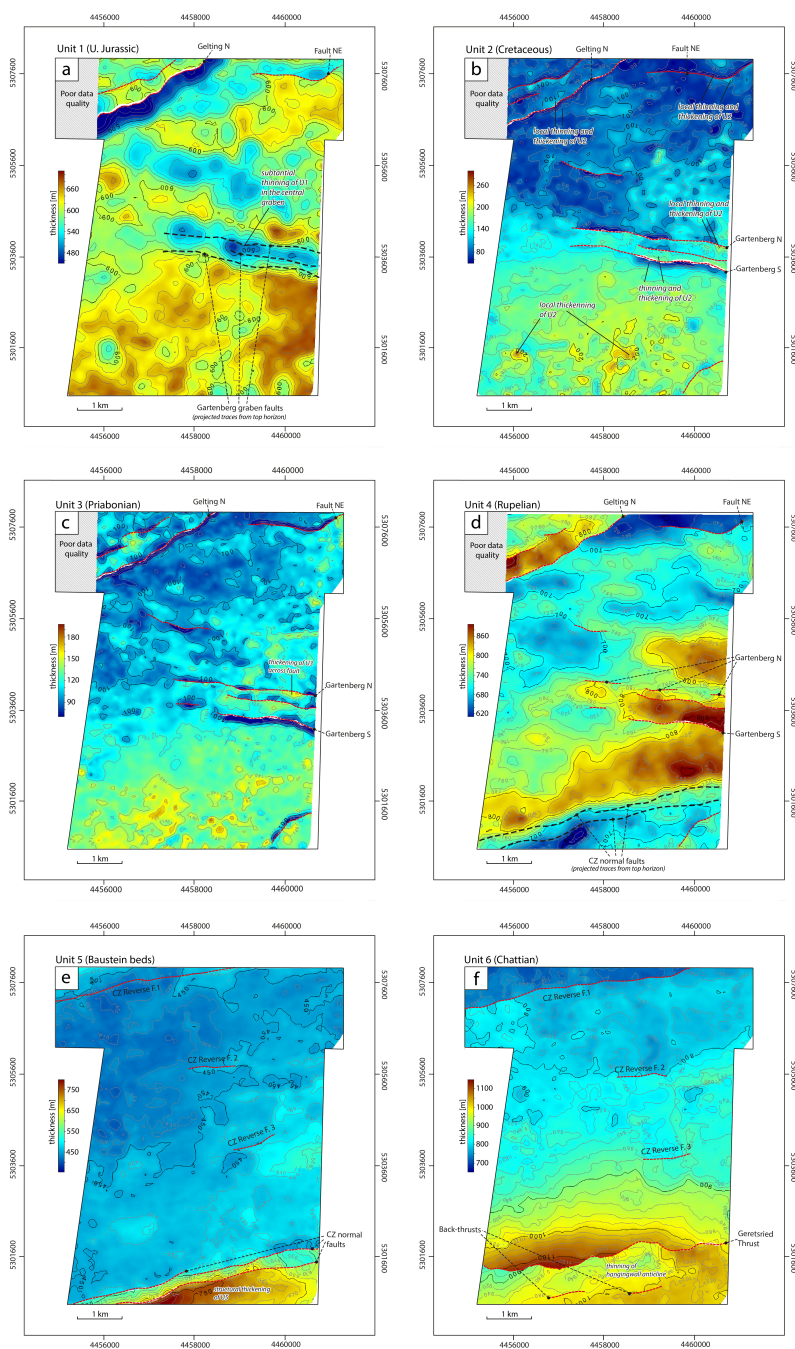


Figure 14. Isochore maps of the five stratigraphic units depicting sediment thickness changes and syn-kinematic growth strata. (a) Unit 1 (carbonate platform; Oxfordian to Early Berriasian); (b) Unit 2 (Valangian-Hauterivian marl, Gaultian sandstone, Turonian marl; Valangian to Turonian); (c) Unit 3 (Basal sandstone, Lithothamnion limestone; Priabonian); (d) Unit 4 (Rupelian clay; Rupelian); Unit 5 (Baustein beds; Late Rupelian–Early Chattian); (f) Unit 6 (Chattian sandstones; Chattian). Note that the thickness minima on the footwall of the faults on thickness maps of Units 2 and 3 are not stratigraphic in origin, but are computational artefacts associated with the fault gap on top surface. See text for discussion.

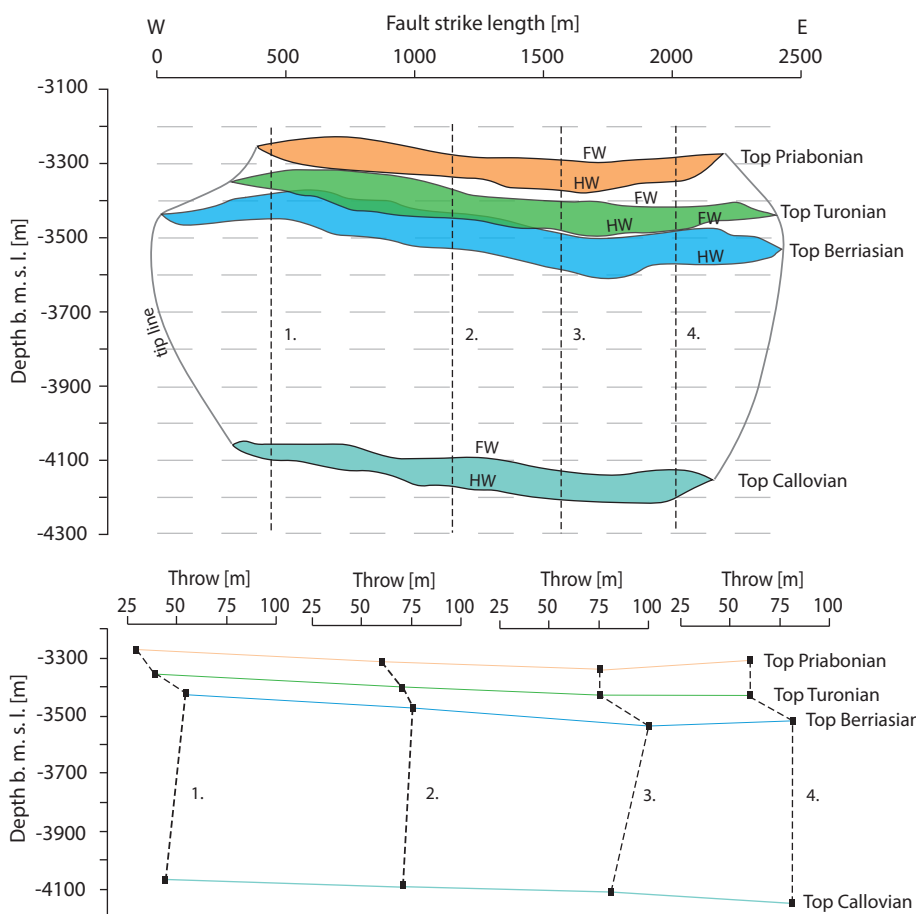


Figure 15. (a) Allan map and (b) t - z plot for Fault NE. Note that the throw decreases from top Berriasian stratigraphically upwards and downwards. The cut-offs of the horizons form a near-elliptical shape. Locations of t - z profiles are shown in a). Footwall and hanging-wall cut-offs are abbreviated FW and HW, respectively.

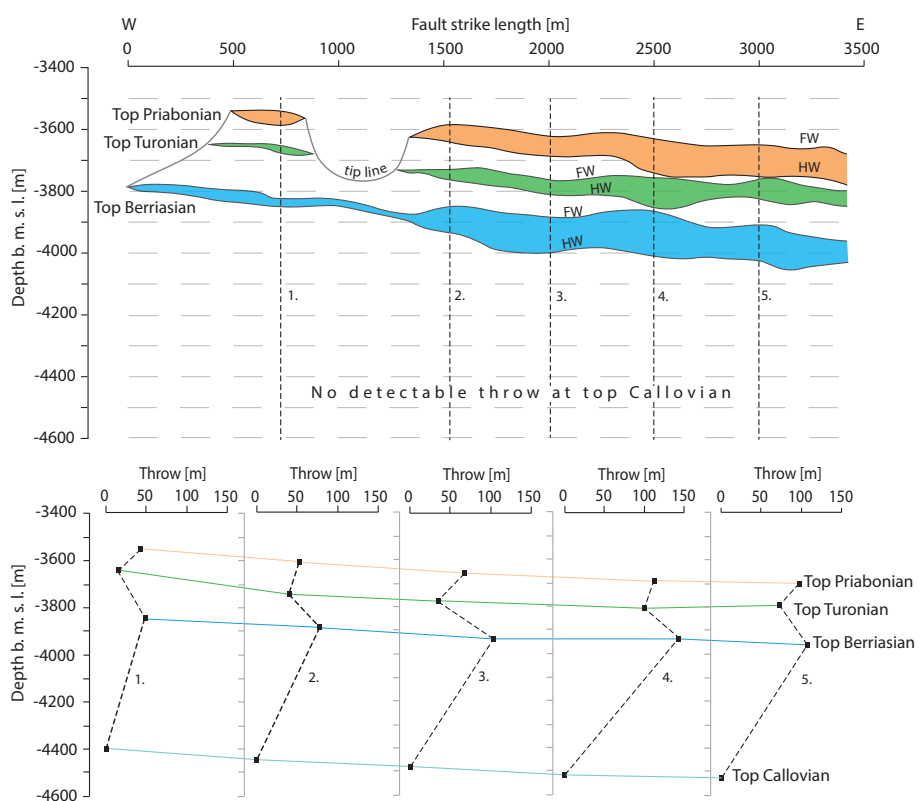


Figure 16. (a) Allan map and (b) t - z plot for Fault Gartenberg S. The cut-off polygons show upward bifurcation of Fault Gartenberg S. Note throw reduction at top Turonian. Footwall and hanging-wall cut-offs are abbreviated FW and HW, respectively.

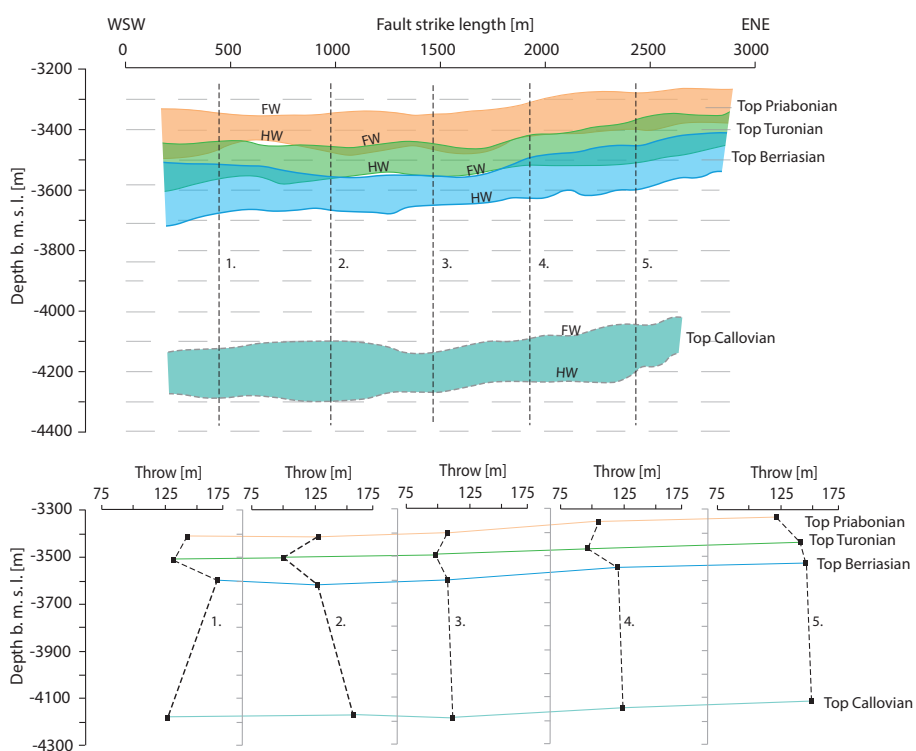


Figure 17. (a) Allan map and (b) t - z plot for Fault Gelting N. The throw distribution shows no significant throw variations along the displaced horizons. Footwall and hanging-wall cut-offs are abbreviated FW and HW, respectively.

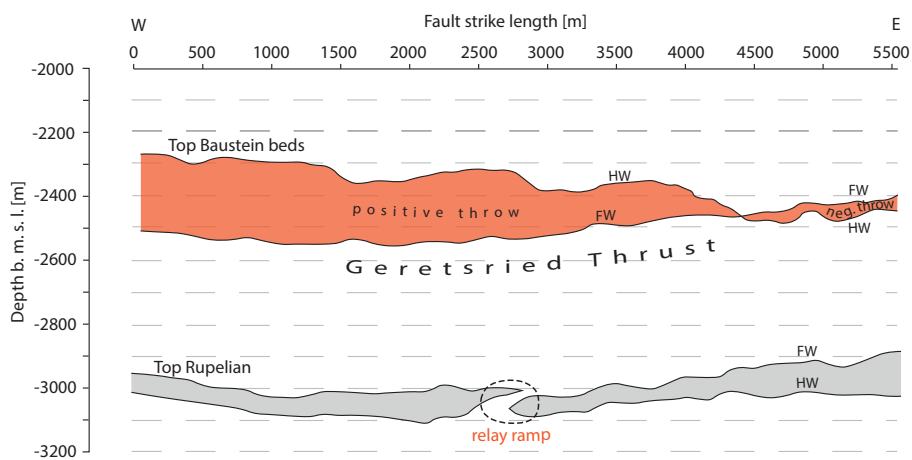


Figure 18. Fault cut-off map of the Geretsried Thrust at top Baustein beds (red) and of the underlying normal faults at top Rupelian (grey). Note substantial decrease of throw on the Geretsried Lower Thrust to the E. See text for discussion. Footwall and hanging-wall cut-offs are abbreviated FW and HW, respectively.

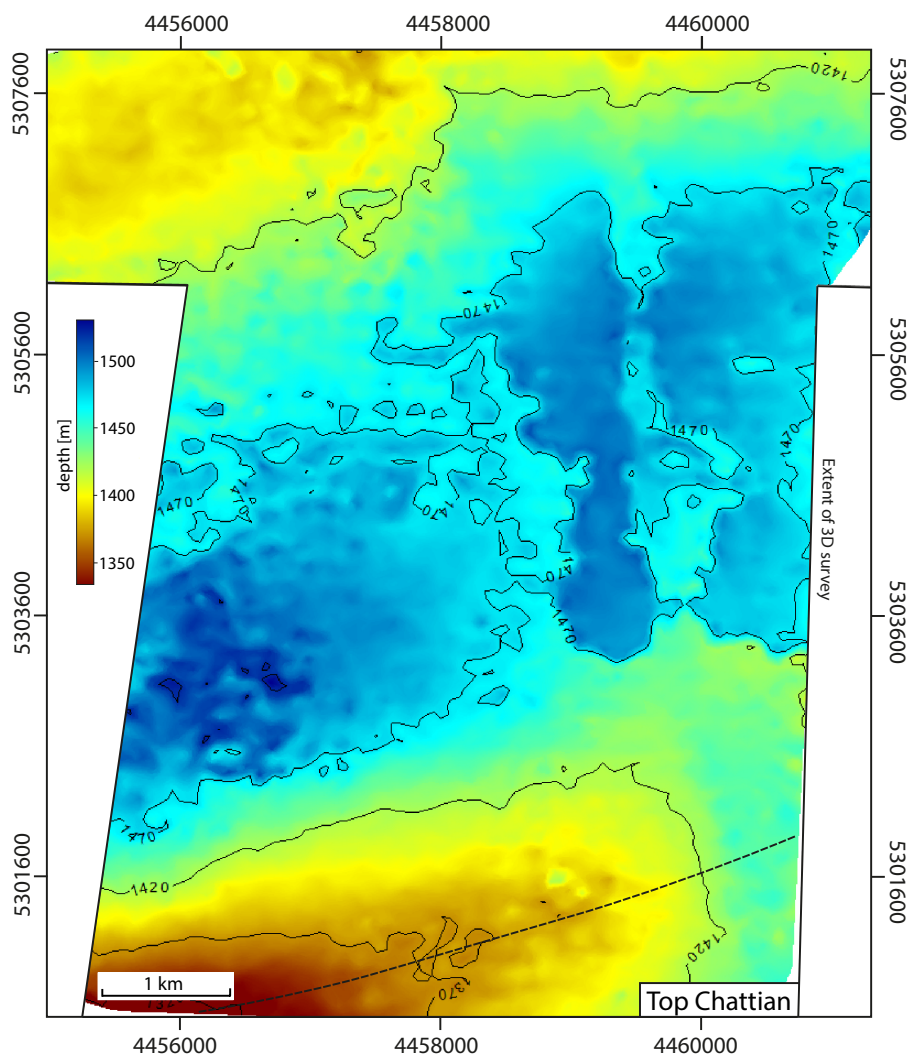


Figure 19. Depth-structure map of top Chattian showing termination of the Geretsried fold to ENE. Dashed line represents the fold hinge. No faulting occurs at this level.

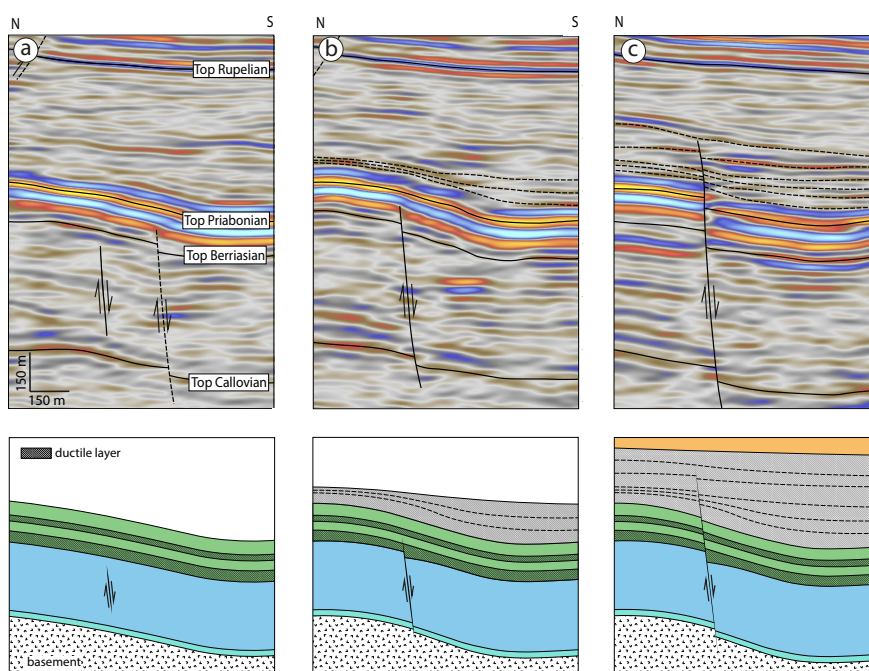


Figure 20. Stages of lower fault evolution based on the example of Fault NE: a) Nucleation of Fault NE within the carbonate platform; b) Up-dip propagation of the fault inhibited by multi-layered stratigraphy. Overlying units are forced to flex; c) Eventually, the fault breaches the monocline. The stagnant fault tip is buried by the later Rupelian sediments.